Thermodynamics of ordering and mixing in plagioclase feldspars: atomistic modelling in favour of Landau theory

Benoît Dubacq

Contributions to Mineralogy and Petrology manuscript No.
(will be inserted by the editor)

Thermodynamics of ordering and mixing in plagioclase feldspars: atomistic modelling in favour of Landau theory

Benoît Dubacq

Received: 20 May 2022 / Accepted: 27 September 2022

Abstract Plagioclase feldspars are key components of terrestrial planets and deriving their phase diagram and activity-composition relations has been the subject of many studies. Three main approaches have been used for thermodynamic modelling of the behaviour of plagioclase feldspars, and all three broadly disagree in terms of the magnitude and relative importance of mixing energies and ordering energies.

This study uses Monte-Carlo simulations based on classical atomistic modelling to provide independent constraints over ordering and mixing for anorthite and along its solid solution with albite.

Unsurprisingly, Al avoidance plays a key role. The competition between first-neighbour and second-neighbour interactions is highlighted, providing simple explanations to the high degree of short-range order in macroscopically-disordered plagioclase. The mixing properties obtained in this study support strong non-ideality, with negative mixing enthalpy and temperature-dependent mixing entropy. Ordering energies are consistent with studies using Landau theory. Unfortunately the form of the Landau equations hindered parametrisation of a full thermodynamic model from albite to anorthite, even though the thermodynamic formalism remains simple. Reasons, perspectives and implications for the phase diagram of ternary feldspars are discussed.

Keywords Plagioclase · Landau theory · atomistic modelling · ordering · Al-avoidance

1 Introduction: thermodynamic modelling of plagioclase feldspars

Plagioclase feldspars are major constituents of the crust of terrestrial planets and their satellites, including Earth, the Moon, Venus and Mercury (e.g., Namur et al., 2011; Fegley et al., 1992; Namur and Charlier, 2017). Composition variations along the albite (ideally

B. Dubacq
Sorbonne Université, CNRS-INSU
Institut des Sciences de la Terre de Paris, ISTeP UMR 7193
Tour 46-00, 3ème étage, case 129
75005, Paris, France
Tel.: +33 (0)1 44 27 51 01
https://orcid.org/0000-0001-6927-0656
E-mail: benoit.dubacq@sorbonne-universite.fr

$NaAlSi_3O_8$) to anorthite (ideally $CaAl_2Si_2O_8$) solid solution depend on pressure-temperature conditions of crystallisation, making plagioclase a key mineral for reconstruction of pressure-temperature paths of high-grade metamorphic rocks as well as of the evolution of magmatic rocks.

Within this solid solution, cation exchange ($Na^+ + Si^{4+} = Ca^{2+} + Al^{3+}$) takes place into minerals with different structures and mutually incompatible Al-Si ordering patterns. Deriving a complete phase diagram for plagioclase has been a challenging task and the version proposed by Carpenter (1994) has not been significantly modified. The low-temperature part remains mysterious as the incommensurately modulated '*e*' structures and their thermodynamic stability are poorly understood, although evidence for the low-temperature closure of the Bøggild gap is growing (Jin and Xu, 2017; Jin et al., 2021). The main features of the phase diagram at lithospheric temperatures are briefly outlined below and the reader is referred to Carpenter (1994) for more details.

Phase transitions within solid solutions are of primary importance in silicates but complicate thermodynamic modelling. Three main modelling approaches have been followed for plagioclase feldspars:

- assuming a continuous solid solution and discarding phase transitions (e.g., Ghiorso, 1984; Benisek et al., 2004, 2010; Namur et al., 2012), using a non-ideal mixing model to reproduce calorimetric and/or phase equilibrium constraints.
- treating each structure as separate solid solutions (one solid solution for $C\bar{1}$, one for $I\bar{1}$). This requires four end-members, two of which are virtual (i.e. $C\bar{1}$ anorthite and $I\bar{1}$ albite, forming 'Darken's quadratic formalism', see Holland and Powell, 1992). The transition from one structure to the other follows the structure with the lowest Gibbs energy.
- using the 'true' end-members in their equilibrium state and adding an energetic cost linked to ordering. Carpenter (1988) has shown that Landau theory, which provides a theoretical framework for phase transitions, may be parametrized on the basis of calorimetric measurements to do so.

Holland and Powell (1992) have compared the second and third approaches to conclude that the approach based on Landau theory does not perform as well as Darken's quadratic formalism. Using phase equilibria experiments (in particular from Elkins and Grove, 1990) and cation-exchange data (Orville, 1972; Schliestedt and Johannes, 1990), Holland et al. proposed activity models relying on near-ideal mixing between albite and anorthite, with $W_{G\mathrm{Ab-An}} \sim 0$ at 1300°C in the most recent model with ASF (ASymmetric Formalism; Holland and Powell, 1992, 2003; Holland et al., 2022). In agreement, the small volume difference ($\sim 0.3\%$) between high albite and anorthite suggests symmetric mixing and meets the criteria set by Kerrick and Darken (1975) for ideality.

But in a critical review of the experiments of Elkins and Grove (1990), Benisek et al. (2010) retrieved a mixing model based on calorimetry, using non-ideal mixing between albite and anorthite, with large and positive mixing enthalpy and entropy resulting in $W_{G\mathrm{Ab-An}} = 14$ and $W_{G\mathrm{An-Ab}} = 6$ kJ (also at 1300°C). This derivation assumes generalized disordering and gives a good fit to natural samples, yielding much lower K content in plagioclase (approaching zero above An_{60}) and lower Ca content near the orthoclase end-member. Authors suggest that their model is superior because it is based on more direct measurements of the mixing properties. Yet, the earlier work using Landau theory (summarised by Carpenter, 1994) parametrised on the basis of structural measurements and calorimetry also offers a very different perspective, where mixing is very non-ideal, with large, negative and asymmetrical mixing enthalpy along albite-anorthite combined to large ordering enthalpy for

anorthite. The non-ideality parameters of Carpenter (1992) in the $C\bar{1}$ domain at 1300°C are $W_{G\mathrm{Ab-An}} = -82$ and $W_{G\mathrm{An-Ab}} = 4$ kJ.

Striking inconsistencies remain between these models. This contribution aims at providing independent constraints on the thermodynamics of ordering and mixing in anorthite and its solid solution with albite. A classical Monte-Carlo simulation approach was selected for its flexibility and applicability to structures sufficiently large to model short and long-range ordering, building on previous work such as the two-dimensional model of Vinograd and Putnis (2001). Emphasis is placed on linking cation distribution to mixing properties. The enthalpy and configurational entropy of ordering are evaluated along the albite-anorthite solid solution and compared to models using Landau theory.

Below, the anorthite content of plagioclase is reported as $X_{\mathrm{Ca}} = \frac{\mathrm{Ca}}{\mathrm{Ca+Na}}$. X_{An} and X_{Ab} represent the thermodynamic mole fractions used as ideal activities of the anorthite and albite end-members.

2 Albite to anorthite: ordering and phase transitions within a solid solution

Albite and anorthite have three-dimensional framework structures, shown in Fig. 1 emphasizing tetrahedra. Albite is monoclinic ($C2/m$ structure) above 978°C and triclinic below (Fig. 1 A: $C\bar{1}$ structure from Harlow and Brown, 1980), with four tetrahedral (T) sites noted T1o, T1m, T2o and T2m (o standing for original and m for mirror). Anorthite is triclinic with $I\bar{1}$ structure above ∼200°C and $P\bar{1}$ below (Fig. 1 B from Angel et al., 1990), with 16 T sites, 8 of T1 type and 8 of T2 type. The labelling in Fig. 1 B) is that of Angel et al. (1990) and allows distinguishing between 'i' sites becoming equivalent under $I\bar{1}$ symmetry and 'z' sites becoming equivalent under $C\bar{1}$ symmetry. In the albite-anorthite solid solution, the temperature of the $C\bar{1} \rightleftharpoons I\bar{1}$ transition increases linearly with anorthite content and extrapolates to ∼2320°C for anorthite (above its melting point, Carpenter and McConnell, 1984).

Many studies have shown that these phase transitions are linked to Si-Al ordering and particularly 'Al avoidance' – where Al atoms are located as far from one another as possible, keeping energetically costly Al-O-Al bonds to a minimum.

The $P\bar{1} \rightleftharpoons I\bar{1}$ transition is displacive (Carpenter, 1988; Angel et al., 1990), and the arrangement and linkages of the tetrahedra is identical in $P\bar{1}$, $I\bar{1}$ and $C\bar{1}$ feldspars as shown in Fig. 1. Each T site has four first-neighbour tetrahedra, each of these connected to three more tetrahedra, but there are only 10 (not 12) second-neighbour tetrahedra as two of the second-neighbours are linked to the same first-neighbours (Fig. 1C). Normalising to the usual AT_4O_8 basis, with A the Ca-Na site, the arrangement of the 4 tetrahedra, with 4 first-neighbours each, yields a total of 8 pairs of first-neighbours (i.e. 8 T-O-T bonds) per formula unit (p.f.u.). Similarly, the 40 second-neighbours p.f.u. make 20 second-neighbour linkages p.f.u.

The pattern of Al occupation is fundamentally different between the ordered varieties of feldspars. Al occupies almost exclusively T1o in low albite but it is evenly distributed between the T1 and T2 subtypes in ordered anorthite. There are no Al-O-Al bonds in either case: in ordered anorthite each Al atom has 4 Si neighbours ($n_{\mathrm{Si-O-Al}} = 8$ p.f.u.), ordered albite has 4 Si-O-Al and 4 Si-O-Si bonds p.f.u. The number of second-neighbour Al-Al pairs increases from 0.5 p.f.u. in low albite (as T1o has only one T1o out of 10 second neighbours, Fig. 1C) to 10 p.f.u. in ordered anorthite (half the 20 linkages p.f.u.). Disordered varieties also differ: fully disordered albite has 0.5 Al-O-Al, 3 Si-O-Al and 4.5 Si-O-Si bonds p.f.u. on average, fully disordered anorthite has 2 Al-O-Al, 4 Si-O-Al and 2 Si-O-Si bonds p.f.u.

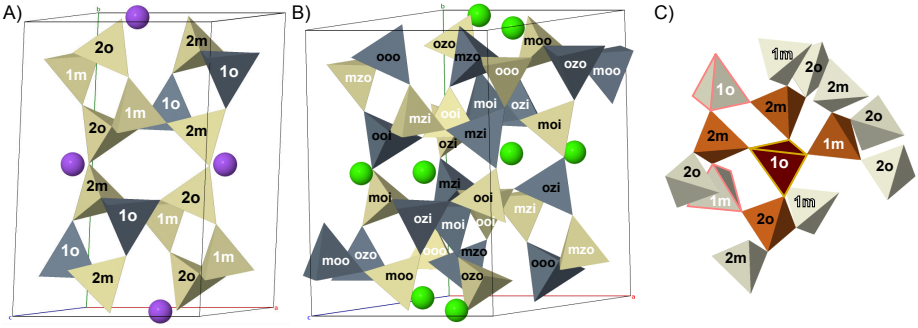

Fig. 1 Structures of $C\bar{1}$ albite (A, after Harlow and Brown, 1980) and $P\bar{1}$ anorthite (B, after Angel et al., 1990), showing unit cells. Tetrahedra of T1 type are labelled in white, in black for T2 sites. The labelling is kept to a minimum for readability. In ordered albite and anorthite, gray tetrahedra are filled with Al, pale yellow tetrahedra with Si. Note that there are no Al-O-Al bonds in either case, and no Al-Si second-neighbours in anorthite. Sodium is purple in A and calcium green in B. C Local environment of a T1o tetrahedron (dark red), with four tetrahedra as first-neighbours (brown) and ten as second-neighbours (pale beige). Note the two tetrahedra with pink edges, each connecting two first-neighbours to the central T1o. C) applies to albite, anorthite and their solid solution. Oxygen atoms not depicted. Drawn with the help of Jmol (http://www.jmol.org/).

on average. These values represent random Al-Si distribution, possibly never met in nature even for high albite (Prewitt et al., 1976) and certainly not for anorthite (Phillips et al., 1992).

Consequently, disordering affects the nature of first and second neighbours differently with varying anorthite content. If neighbouring Al and Si atoms are allowed to swap positions to model disordering, in albite the number of second-neighbour Al-Al pairs increases before that of Al-O-Al bonds: for example exchanging Al in T1o with Si in T2o results in one additional second-neighbour Al-Al pair, but no Al-O-Al bonds. In anorthite, disordering will necessarily increase Al-O-Al bonds and decrease second-neighbour Al-Al pairs, meaning that the energetic penalty of creating Al-O-Al bonds will be modified by the joint disappearance of Al-O-T-O-Al linkages. For example, a single exchange of neighbouring Si and Al creates three Al-O-Al bonds but decreases the number of second-neighbours Al atoms by 10. This competition effect is significant for disordering of plagioclase feldspars as second-neighbour interactions are numerous, even though about ten times less energetically costly than first-neighbour interactions (e.g., Vinograd et al., 2001; Bosenick et al., 2001, and this study).

An order parameter Q_{od} is generally used to estimate the state of Al-Si ordering, but the mutually incompatible ordering patterns of albite and anorthite complicate defining an order parameter for their solid solution. Here, the definition of Angel et al. (1990) is retained for albite and anorthite: $Q_{od} = < Al >_{Al} - < Al >_{Si}$, with $< Al >_{Al}$ the average occupancy by Al of the Al-rich sites and $< Al >_{Si}$ the average occupancy by Al of Si-rich sites (see Fig. 1A-B). In randomly-disordered albite and anorthite, Q_{od} is zero. In anti-ordered anorthite (with Al occupying all of the Si sites and Si in the Al sites), $Q_{od} = -1$; if Al was to occupy a Si site in albite, Q_{od} would be $-1/3$. Q_{od} is an average, "macroscopic" parameter and $Q_{od} = 0$ does not necessarily imply random cation distribution as short-range order may remain.

Other schemes may be used to estimate the ordering state, such as the difference between Al occupancy of the T1 sites for albite (a measure of $C\bar{1}$ ordering, here noted Q_{od}^{Ab}, see e.g. Salje, 1985; Salje et al., 1985; Tribaudino et al., 2018; Kroll et al., 2020). Q_{od}^{Ab} applies to K feldspar (e.g., Holland and Powell, 1996) but is ill-suited to anorthite because $Q_{od}^{Ab} = 0$

in both ordered and randomly-disordered anorthite. Holland et al. (2022) combine Q_{od}^{Ab} to a $Q_t = X_{Al}^{T1} - X_{Al}^{T2}$ parameter, obtaining $Q_{od}^{Ab} = 0$ and $Q_t = 1$ for ordered anorthite with their 2Q model. However, this is inconsistent with the ordering pattern of anorthite (Fig. 1B where $Q_t = 0$) and implies Al-O-Al bonds through T1-T1 linkages, following erroneous site repartition for their ordered anorthite end-member 'oan'.

Here Q_{od} is only evaluated for end-members because site occupancies could not be strictly defined for the ordered varieties with intermediate composition.

The temperature-dependence of the $I\bar{1} \rightleftharpoons P\bar{1}$ and $C\bar{1} \rightleftharpoons I\bar{1}$ transitions for anorthite-rich plagioclase and previous work on anorthite show that these phase transitions are essentially tricritical in character, yet there has been fluctuations around the exact order of the phase transitions. Carpenter (1988) suggested that these transitions become second-order if a small amount of Na is incorporated, consistent with changes of the Al-Si order state inherited from crystallisation or heat treatment. It has been subsequently noted that a first-order approximation for anorthite, becoming tricritical with increasing Na content, gives a much more favourable fit to the measured degree of ordering (Carpenter, 1988; Angel et al., 1990; Carpenter, 1992, 1994). Salje (1987) and Redfern and Salje (1987) provide further explanations at lattice and Brillouin zone scale for this behaviour, which remains in favour of the essentially tricritical character of these transitions.

3 Atomistic modelling

Atomistic modelling with the J_s approach has been selected as it is well suited to the problems of cation ordering and solid solutions, allowing fast Monte-Carlo simulations over structures containing thousands of atoms and bringing constraints at the resolution required to petrology (e.g., Lanari and Duesterhoeft, 2018). The method is thoroughly reviewed and detailed by Dove (2001) and Bosenick et al. (2001). Twenty years after these reviews, computing capacities have dramatically increased and Monte-Carlo simulations are much less time-consuming, but the method remains cumbersome and has not been applied extensively to feldspars as research efforts have been devoted to other systems since the early 2000's.

3.1 The J_S method

The J_s method attributes an energetic cost to selected bonds or cation neighbours: excess energies are then estimated from the number of these bonds or neighbours. This approach results in simplifications and requires a set of interaction parameters (the J_s) specific to each structure and composition; yet it has successfully reproduced ordering in many silicates and has been adapted in various ways. Each J represents the energy of an interaction – between Al atoms through Al-O-Al linkages for example – then interactions are summed and added to a reference energy level (see Eq. 1 below). During the Monte-Carlo simulations, the structure is fixed and neither strain nor phase transitions are modelled, but the J_s may include a strain energy component. Bosenick et al. (2001) report a compilation of J_s for a number of silicates, including albite and anorthite (from Myers, 1999).

Vinograd and Putnis (2001) provide a simplified model using two values of J_s (one for first neighbour Al-Al J_{Al-Al}^{1st}, one for second neighbour Al-Al J_{Al-Al}^{2nd}) on a flat (two-dimensional) grid analogue of feldspar with varying Si/Al ratio. The Js were fitted to experimental results and to the modelling results of Myers (1999), resulting in $J_{Al-Al}^{1st} \sim 40$ kJ/mol (0.4eV pfu) for anorthite. Scaling the results of Myers (1999) for albite gives $J_{Al-Al}^{1st} \sim 57.2$

kJ/mol and $J^{2nd}_{Al-Al} = 9.2$ kJ/mol, but Vinograd and Putnis (2001) argue that a larger value of J^{2nd}_{Al-Al} ($\sim$21 kJ/mole) is necessary to stabilize long-range order in albite. However, application of this approach is limited as the connections of albite tetrahedra differ from the flat analogue of Vinograd and Putnis (2001) where each T site has 4 first-neighbours and 8 second-neighbours instead of 10. Consequently the flat analogue precludes modelling the preference of Al for the T1o site, an important feature of albite disordering (Kroll et al., 2020). It is noted that the cluster variation method, a statistical model presented in detail by Vinograd and Putnis (1999), has given an excellent fit to phase transitions in feldspars (Vinograd et al., 2001).

Here the GULP software (Gale, 1997; Gale and Rohl, 2003, v. 5.1) has been used to calculate the energy level for a large number of plagioclase structures with different cation distributions and compositions. Large cell sizes are necessary to model disordered and partly-ordered structures. The set of J_s includes first- and second-neighbour Al interactions, namely Al-O-Al bonds and Al-O-T-O-Al linkages, in addition to Ca-Si and Na-Ca interactions for the $C\bar{1}$ solid solution. The J_s are estimated via fitting of the GULP energies after counting the number of each bond type in each structure with dedicated code. The procedure is similar for $P\bar{1}$ anorthite and the $C\bar{1}$ solid solution, using energy minimization over primitive unit cells and larger replicates of the unit cell (supercells) to allow disorder. The use of supercells releases space group symmetry constraints, allowing deformation of bonds when compared to the ordered structure. A $2 \times 2 \times 2$ supercell of albite is larger than 14 Å in every direction, a value in the range of or larger than the diameter of the strain field around a single defect, which varies depending on the mineral, site and defect type. Authors argue this length is around 9 Å for Ti in quartz, at least 20 Å for K in albite, and $\sim$ 16 Å for La in oxide perovskite (see e.g. Hayward and Salje, 1996; Carpenter et al., 2009, and references therein). It is noteworthy that strain decreases very quickly away from point defects (e.g., Dubacq and Plunder, 2018; Figowy et al., 2020, 2021), and that setting a hard limit to the strain field is somewhat arbitrary.

3.2 Choice of potentials

Interatomic potentials (Table 1) are from Lowitzer et al. (2008) and Sainz-Diaz et al. (2001). This set of potentials originates mostly from the study of Winkler et al. (1991) and has been refined to give excellent fits to many silicate structures (e.g., Bosenick et al., 2001; Vinograd and Sluiter, 2006; Vinograd et al., 2007, 2011; Dubacq et al., 2011), including albite as emphasized by Lowitzer et al. (2008).

3.3 Derivation of the J_S

Albite and the $C\bar{1}$ albite-anorthite solid solution A set of 1081 GULP simulations has been used to constrain the J_s along the $C\bar{1}$ albite-anorthite solid solution. Ordered albite (with Al in T1o) has the lowest energy, with zero Al-O-Al and 0.5 second-neighbour Al atoms p.f.u. For albitic configurations with Al occupying other T sites (T1m or T2o or T2m), the numbers of Al-O-Al and Al-O-T-O-Al remain unchanged but these configurations have higher energies, justifying the need to distinguish between T sites.

Larger cells were used to model structures with varying degrees of order to ensure that a large range of configurations were sampled, including partially ordered structures, structures

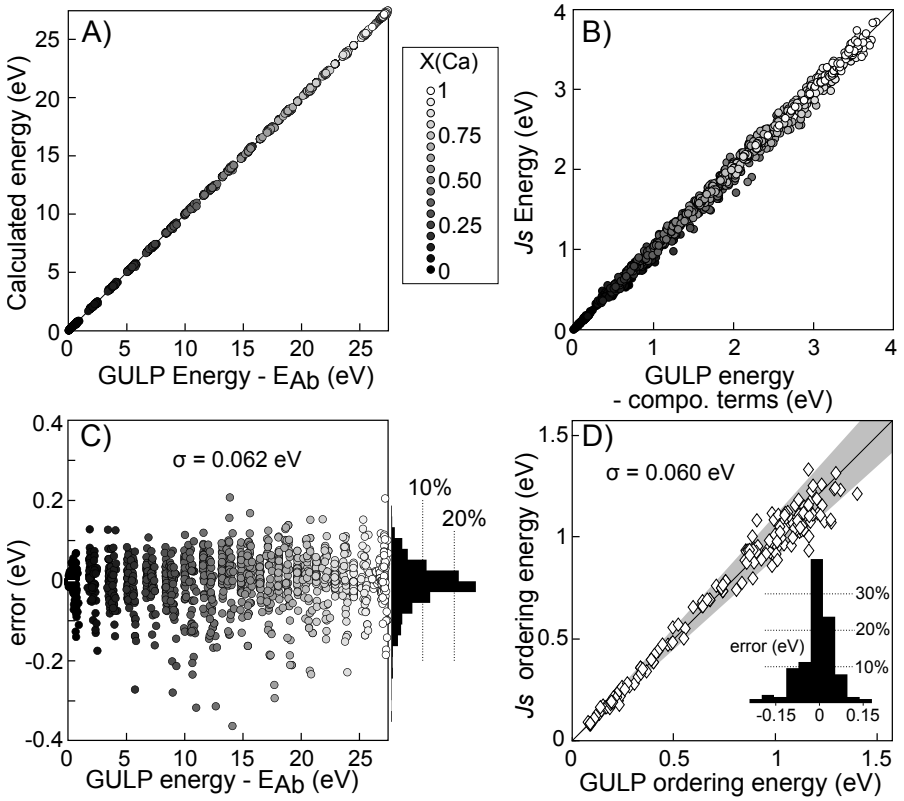

Fig. 2 Quality of the fit between energy values calculated with GULP and with the J_s shown in table 2 for variously-ordered $C\bar{1}$ structures along the Na-Ca solid solution (A to C) and for $P\bar{1}$ anorthite (D). All energy values are expressed p.f.u. A) Comparison of energies relative to that of albite (E_{Ab}). B) Comparison of the energy contribution from the J_s compared to GULP energies to which composition-dependent terms have been removed. C) Residual error and its distribution (right-hand side). D) $P\bar{1}$ anorthite: comparison of calculated energies relative to that of ordered anorthite. The grey field shows the domain below 10% error. The distribution of the residual error is given in inset.

with ordered and anti-ordered domains, and disordered structures with random Si-Al distribution. Configurations that are energetically very unfavourable (with many Al-O-Al bonds) have also been sampled to evaluate first-neighbour interactions, as well as less unfavourable structures containing many second-neighbour Al-Al with as little Al-O-Al as possible, to properly evaluate second-neighbour interactions.

The following equation was used to describe the energy E of variously ordered plagioclase feldspars:

$$E = E^0_{\mathrm{Ab}} + X_{\mathrm{Ca}}\Delta E^0 + (X_{\mathrm{Ca}}\,(1 - X_{\mathrm{Ca}}))\,W + \Sigma M J_s \tag{1}$$

where E^0_{Ab} is the reference energy level, chosen as that of ordered albite (the lowest), ΔE^0 is the linear energy variation with the $Na^+ + Si^{4+} \rightleftharpoons Ca^{2+} + Al^{3+}$ exchange, W is a Margules-type term for non-linear energy variation along that exchange vector, and M is a matrix containing the number of neighbours with corresponding J_s energies. This approach is similar to that of many studies (Vinograd and Sluiter, 2006, for example), where there is a set of J values for each neighbour type. Here a set of three types of neighbours is necessary, for

convenience Al-Al (first and second neighbours), Ca-Na and Ca-Si interactions were chosen. The J_s for Al-Al interactions were first estimated for albite where there are no Ca-Na and Ca-Si neighbours, via minimisation of the squared relative difference to the GULP energies using the Levenberg-Marquardt algorithm Marquardt (1963) rather than least-square regression to ensure structures with small ordering energies (e.g. containing Al-Al as second- but not first-neighbours) were well reproduced. From this set of values, the whole set of parameters was optimized, allowing the first-neighbour Al-Al J_s to vary linearly with composition. Values for $J_{\mathrm{Ca-Si}}$, ΔE^0 and to a lesser extent W are correlated. As the physical relevance of W is unclear in this context, the whole procedure including Monte-Carlo simulation was carried out with $W = 0$ for $X_{\mathrm{Ca}} = 0.5$, 0.75 and 1 to ensure that adding this parameter did not result in significantly different excess mixing energies. As similar mixing energies were obtained, the set of optimised values including W was selected because it yielded a slightly better misfit and with lower values for some of the J_s.

The resulting set of parameters is provided in Table 2 and the quality of the fit is shown in Fig. 2 A-C. The misfit appears better for albite, anorthite and close to end-members than within the solid solution but the spread was considered acceptable because there is no systematic pattern of errors (Fig. 2 C). Values for first-neighbour $J_{\mathrm{Al-Al}}$ decrease with anorthite content, consistent with the results of Bosenick et al. (2001) for albite and anorthite. They remain much larger than second-neighbour Al-Al interactions, particularly for those involving T1o as this site is favoured by Al (e.g., Kroll et al., 2020). The Ca-Si interaction is intermediate and positive (unfavourable) as expected from local charge imbalance. In contrast the Ca-Na interaction is slightly negative, favouring Ca-Na neighbours. When plotted according to the median distance between neighbours (Fig. 3), the J_s generally decrease with increasing distance but this is attenuated by the fact that distances vary significantly between second neighbours in particular: for example in the albite structure refinement of Harlow and Brown (1980), T1m connects T1o to two T2o as second neighbours, the closest via Ocm (T2o is ~ 4.5 Å away from T1o), the furthest via Odm (~ 5.7 Å).

Anorthite The same set of interactions between tetrahedral cations as for albite has been selected, and the same procedure and regression analysis have been carried out. The energy is normalised to that of the lowest (ordered anorthite, E^0_{An}), and it is noted that in anorthite the number of Ca-Si neighbours is constant regardless of ordering, therefore $J_{\mathrm{Ca-Si}}$ is unnecessary here and Eq. (1) reduces to: $E = E^0_{\mathrm{An}} + \Sigma M J_s$.

A set of 181 structures optimized with GULP has been used to estimate the parameters listed in Table 2. The starting structure was based on the refinement of Angel et al. (1990) in the $P\bar{1}$ space group, selected over $I\bar{1}$ for modelling simplicity as GULP does not handle $I\bar{1}$ structures as readily.

The resulting set of J_s is provided in Table 2 and the quality of the fit is shown in Fig. 2 D. Overall the error structure is similar to that of the $C\bar{1}$ solid solution, with a standard deviation of 0.06 eV and 87 % of the energies estimated within 10% accuracy.

3.4 Monte Carlo simulation

A Metropolis-like diffusive exchange algorithm has been set up, where tetrahedral cations are randomly allowed to swap places with their first neighbour. The new structure is accepted if the exchange is energetically favourable ($\Delta \mathrm{E} < 0$) or, if unfavourable, with a temperature-dependent probability P such as $P = \exp(-\Delta \mathrm{E}/(k_{\mathrm{B}}\mathrm{T}))$ with k_{B} Boltzmann's constant (see

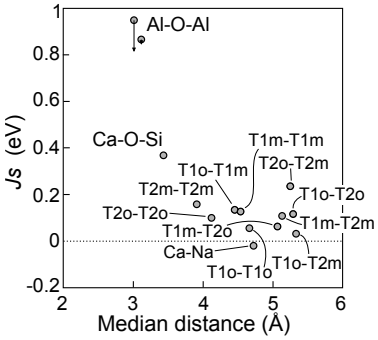

Fig. 3 *Js* for the $C\bar{1}$ solid solution (see Table 2) shown versus median distance between neighbours. First neighbour Al atoms are energetically much more costly than second-neighbour Al atoms. The thin arrow indicates the decrease in $J_{\mathrm{Al-O-Al}}$ from albite to anorthite.

Dove, 2001, for details). This straightforward procedure is not specifically aimed at convergence efficiency or at reproducing precisely diffusion, but allows fast calculations simulating equilibrium. This algorithm has been applied to replicates of the structures in Fig. 1 ($14 \times 7 \times 7$ for anorthite, $14 \times 14 \times 7$ for albite and the $C\bar{1}$ solid solution) containing 5488 formula units ($\sim 110 \times 90 \times 100$ Å). Simulations started from the ordered structure at 0 K and temperature increased in steps of 25 K. Each step comprised either 20 million exchanges or 2 million successful exchanges, depending on which was reached first. Reported energies and numbers of neighbours are averaged over the last 10^5 exchanges.

Along the albite-anorthite solid solution, the exact ordered structure is unknown and must be estimated. To do so, initial structures respecting Al-avoidance were generated from the ordering pattern of anorthite, to which Ca and Al were replaced by Na and Si at random positions to match the desired composition. Annealing was then carried out by repeated heating-cooling cycles between 0 and 1200 K until no lower energy could be found around absolute temperature, also defining smooth excess mixing energy variations with composition. Three cycles were sufficient close to end-members but intermediate compositions around $X_{\mathrm{Ca}} = 0.5$ required up to 15 annealing cycles.

4 Results

Results of the Monte-Carlo simulations are tabulated in Online Resource 1.

4.1 Anorthite

Figure 4 shows the evolution of ordering with temperature calculated for $C\bar{1}$ and $P\bar{1}$ anorthite.

The number of first- (Fig. 4A) and second-neighbour (Fig. 4B) Al atoms evolve jointly as disordering increases, both showing a step function near the critical temperature (T_c). The number of second-neighbour Al atoms decreases faster than first-neighbours increase.

Figure 4C shows the evolution of Q_{od} with temperature. Q_{od} decreases steeply around T_c and remains around zero above that temperature, although the number of Al-O-Al bonds keeps increasing and that of second-neighbour Al atoms decreasing.

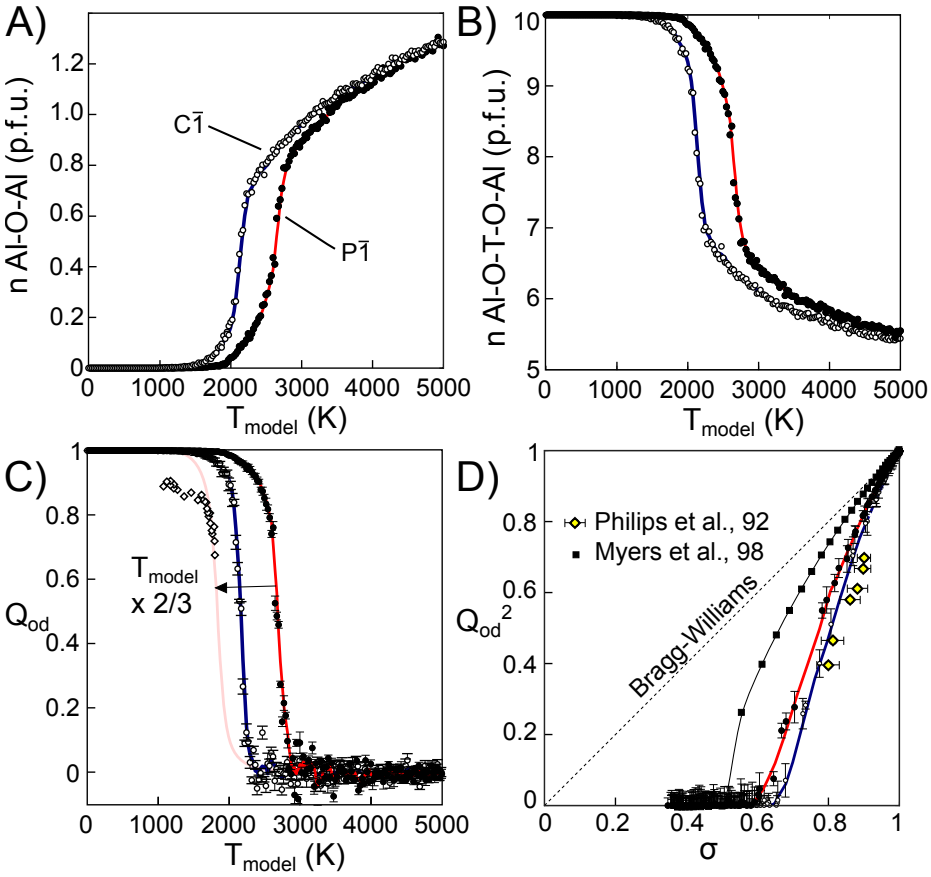

Fig. 4 Results of Monte Carlo simulations on anorthite, starting from the $C\bar{1}$ (open circles, blue curve) and $P\bar{1}$ (closed circles, red curve) structure and using J_s from Table 2. A) number of Al-O-Al bonds, increasing with temperature. B) number of Al-O-T-O-Al (second-neighbour Al-Al interactions), decreasing with temperature. C) Evolution of Q_{od} with temperature, compared to experimental results reported by Carpenter (1992, diamonds). D) Variation of Q_{od} with σ, computed by Bragg-Williams theory, Myers et al. (1998, squares) and the present study (circles), compared to experimental results of Phillips et al. (1992).

As shown in many previous studies, the value for T_c obtained with J_s derived from ab initio techniques is too high, respectively ~ 2200°C and ~ 3000°C for $C\bar{1}$ and $P\bar{1}$ anorthite. Possible reasons for this include algorithmic deficiencies (poor convergence or simplistic diffusion model), overestimated J_s, structural evolution neglected, models remaining below the length scale of coherence of X-ray diffraction, and structures too perfect for comparison with real crystals possibly containing defects such as impurities and dislocations. The J_s being in line with previous studies, overestimation is probably not the main reason for this misfit but cannot be entirely ruled out. A correction factor for the temperatures of $2/3$ provides a much better fit with experimentally-derived values of Q_{od} (in $I\bar{1}$, with which the $P\bar{1}$ results should be broadly consistent). This correction factor is in the high range (i.e. closer to unit value) of factors given by Dove et al. (1996, citing Ashcroft and Mermin (1976)) for the 'adjusted' Bragg-Williams model. The correction factor has been retained thereafter for more realistic temperature estimates (labelled T_{corr} in subsequent figures, as opposed to

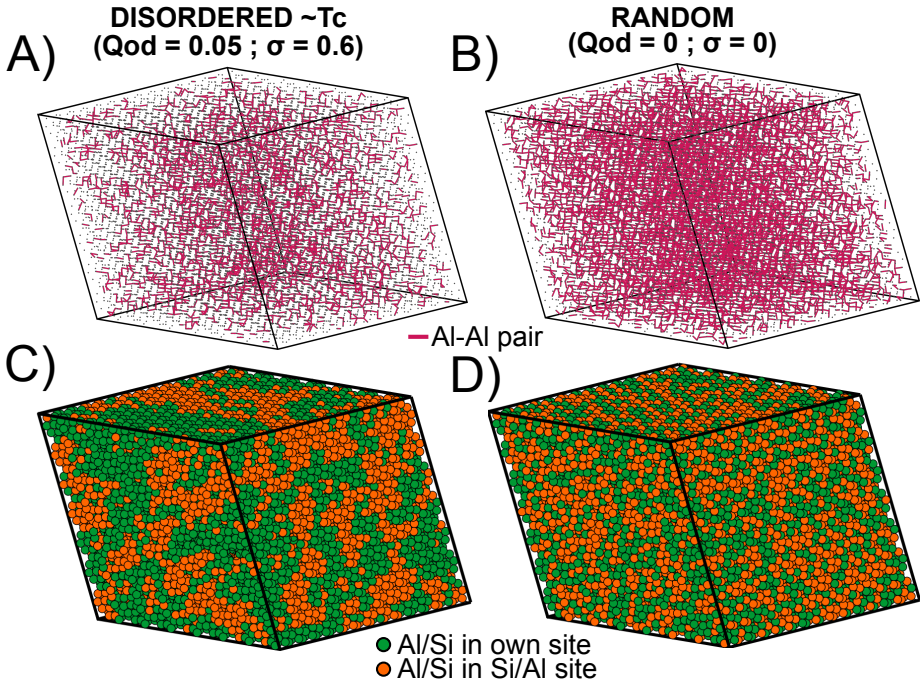

Fig. 5 Results of Monte Carlo simulations on $P\bar{1}$ anorthite, comparing a macroscopically-disordered structure ($Q_{od} \sim 0$) sampled just above Tc to a pseudo-random distribution of tetrahedral cations. The structure with $\sigma = 0.6$ has 0.8 Al-O-Al bonds p.f.u., the random structure with $\sigma = 0$ has 2 Al-O-Al bonds p.f.u. A) and B) highlight first-neighbour Al atoms (crimson segments). C) and D) show sites counting as ordered in green (Al in Al site, Si in Si site) and disordered in orange (Al in Si site, Si in Al site).

T_{model}), affecting the temperature dependency but not the relationships between ordering state and properties such as ordering enthalpy.

The decrease in Q_{od} is compared to the experimental results of Phillips et al. (1992), using their short-range order parameter index σ defined as $\sigma = 1 - n_{Al-O-Al}/2$. The present results are in much better agreement with the NMR data of Phillips et al. (1992) than previous models, a result of the well-defined second-neighbour interactions. Crucially, simulation results are consistent with approximately linear relationship between Q_{od}^2 and σ, with $\sigma \sim 0.7$ when Q_{od} reaches zero. As emphasized by Phillips et al. (1992) and Carpenter (1992), the high degree of short-range order in macroscopically disordered anorthite has implications for the energetic cost of ordering. As discussed below and suggested by Vinograd and Putnis (2001), competition between first- and second-neighbour interactions is a strong control over ordering in feldspars.

Figure 5 compares the ordering state, as approximated by the number of Al-O-Al bonds, of macroscopically-disordered $P\bar{1}$ anorthite with and without short-range ordering. The structure retaining short-range ordering (left) is sampled just above T_c where Q_{od} reaches zero and the number of Al-O-Al bonds is still low ($\sigma \sim 0.6$). It is noteworthy that this structure is just a snapshot of the constantly evolving distribution, in contrast energies and numbers of bonds (Fig. 4) are averaged. For comparison, a structure was generated with a pseudo-random distribution (right) mimicking complete disorder. The number of Al-O-Al

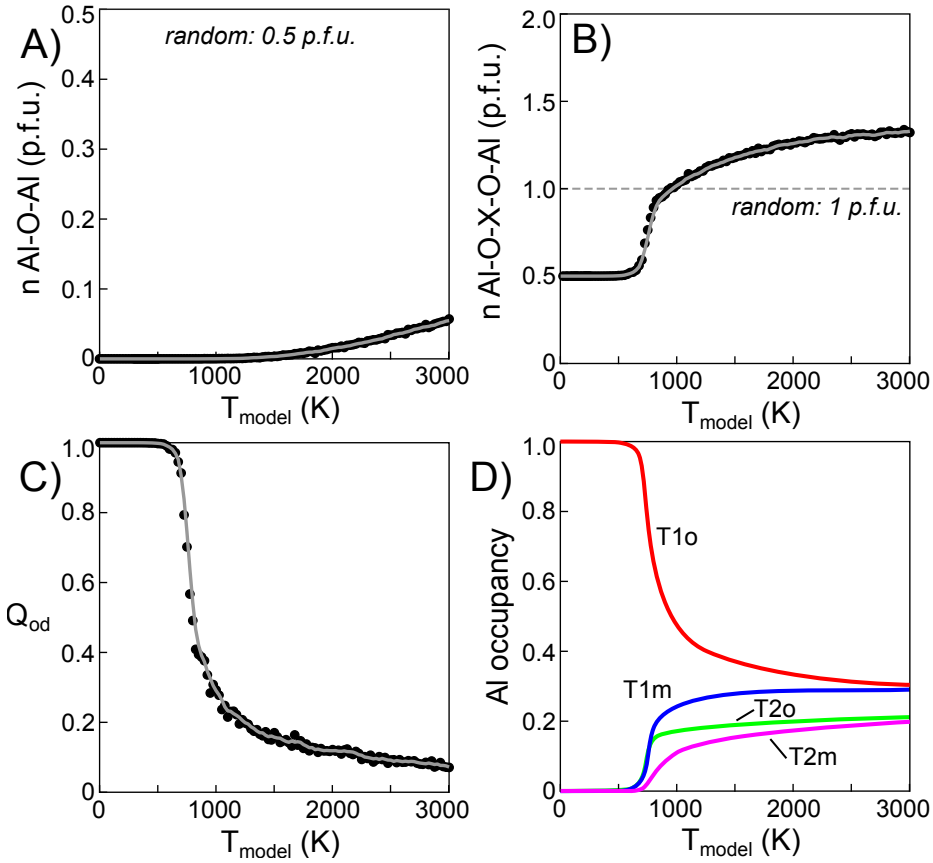

Fig. 6 Results of Monte-Carlo simulations on albite, using J_s from Table 2. A) number of Al-O-Al bonds, increasing with temperature. B) number of Al-O-X-O-Al (second-neighbour Al-Al linkages), increasing sharply around Tc. C) Evolution of Q_{od} with temperature. D) Occupancy of T sites by Al.

bonds are dramatically lower in the structure with short-range order. Overall, as many tetrahedral cations are in their own site (green in Fig. 5C-D) as in the other cation site (orange) in both cases. Yet in the structure with short-range order, anti-ordered micro-domains appear so that the number of Al-O-Al bonds is restricted. The size of these micro-domains is fluctuant and smaller at higher temperature. As shown on Fig. 5, these micro-domains form intricate lenses ∼15 to ∼30 Å long, apparently elongated along the *b* and *c* axes (see Online Resource 2).

4.2 Albite & the $C\bar{1}$ albite-anorthite solid solution

Albite Figure 6 shows the temperature evolution of ordering calculated for $C\bar{1}$ albite. The number of Al-O-Al bonds increases with temperature, very modestly when compared to anorthite (Fig. 4). At $T_{model} = 3000$K, there are less than a fifth of the number of Al-O-Al bonds of randomly-ordered albite. The number of second-neighbour Al atoms increases with temperature (Fig. 6 B), in opposite direction to anorthite, reaching then exceeding the value

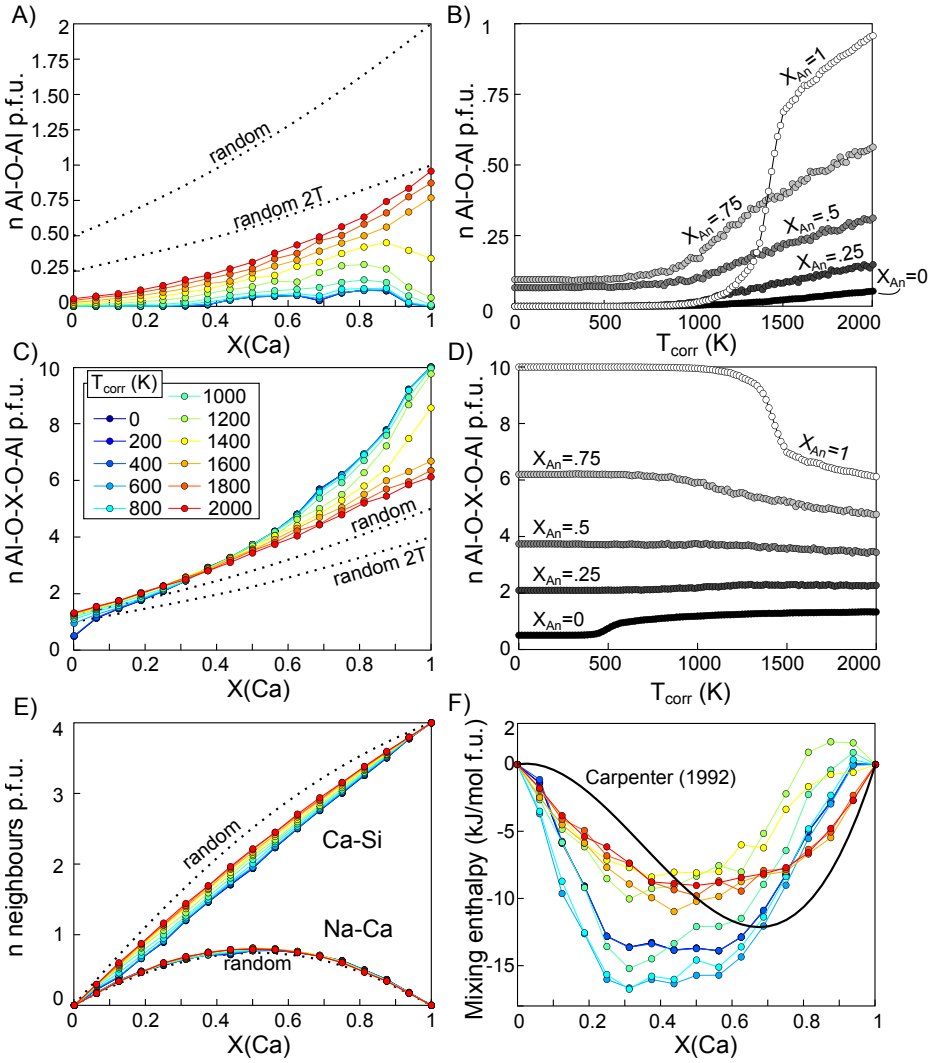

Fig. 7 Results of Monte-Carlo simulation along the $C\bar{1}$ solid solution. The number of bonds expected from random distribution is shown as dotted lines. A) Number of Al-O-Al bonds versus composition, shown for selected temperatures (every 200K). B) Temperature evolution of the number of Al-O-Al bonds for 5 selected compositions. Note that the scale is restricted compared to A). C) Number of second-neighbour Al pairs versus composition for selected temperatures, and in D) versus temperature for selected compositions. E) Number of Ca-Si (top) and Na-Ca (bottom) neighbours versus composition for selected temperatures. F) Mixing enthalpy versus composition for selected temperatures. Colour scales are similar in A-C-E-F and in B and D.

for randomly-ordered anorthite. This increase is strong around $T_{model} = 750K$, at which temperature Q_{od} decreases sharply (Fig. 6C). Yet Q_{od} does not reach zero as abruptly as for anorthite but decreases steadily above this temperature. Average site occupancies are shown in Fig. 6D: Al is entirely located in T1o in ordered albite and favours this site over the entire temperature range. The decrease in T1o occupancy is balanced by increasing Al principally in T1m, then in T2o and T2m. Site occupancies are broadly consistent with ex-

perimental work (Kroll et al., 2020, and references therein) although in the simulations, T2o is preferred over T2m just above T_c, which is interpreted as a bias from the J_s. This suggests that the modelling should be even more heavily parametrised for optimal results, possibly introducing third-neighbour interactions as suggested by Vinograd and Putnis (2001), yet differences are small and therefore will be neglected below.

The $C\bar{1}$ albite-anorthite solid solution The simulated number of first- and second-neighbour Al atoms along the $C\bar{1}$ albite-anorthite solid solution is shown in Fig. 7. Panels A and C also show values expected from random mixing over two or four T sites p.f.u. B and D are selected every 0.25 X_{Ca} and plotted on a restricted scale for readability.

In any case the number of Al-O-Al bonds increases with temperature but remains much smaller than random distribution over the four T sites. This increase is stronger at high anorthite content and sharper (Fig. 7 B). The temperatures at which Al-O-Al bonds increase also vary with composition. The increase is felt at lower temperature around $X_{\mathrm{Ca}} = 0.75$ than at other anorthite content.

Consistent with results for end-members, the number of second-neighbour Al atoms is higher at higher anorthite content for any given temperature (Fig. 7 C and D). At low anorthite content ($X_{\mathrm{Ca}} < 0.4$) the number of second-neighbour Al atoms increases with temperature, but decreases with temperature at higher X_{Ca}. Temperature variations are much sharper for albite and anorthite than for their solid solution (Fig. 7 D).

Between $X_{\mathrm{Ca}} = 0.45$ and 0.85, a small number of Al-O-Al bonds (< 0.1 pfu) is predicted at T = 0K. The number of second-neighbour Al atoms is then slightly lower than expected (possibly by 0.5 pfu, Fig. 7A). As simulations started from the ordering pattern of anorthite without Al-O-Al bonds but with many second-neighbours Al-Al linkages, this is a case where competing first- and second-neighbour interactions favour configurations with a few Al-O-Al bonds rather than many second-neighbour Al atoms. This may also indicate that the simulations have not truly reached equilibrium, despite the annealing cycles.

Figure 7E shows the number of Ca-Si and Ca-Na neighbours. The number of Ca-Si neighbours increases with X_{Ca} and with temperature but remains below the random mixing value, as expected from the relatively high value of $J_{\mathrm{Na-Ca}}$ (Table 2). Accordingly, the number of Ca-Na neighbours appear very slightly above random. Carpenter (1994) favour random mixing of Na and Ca but Jin and Xu (2017) argue that Ca shows a site preference in *e*-labradorite.

The J_s method allows the mixing enthalpy to be estimated within solid solutions. Figure 7F shows that strongly negative mixing enthalpies are obtained for almost all temperatures. In the low ($T_{\mathrm{model}} \leq 800$K) and high ($T_{\mathrm{model}} \geq 2400$K) range of temperatures, the mixing enthalpy appears globally symmetric. In between, the mixing enthalpy appears more negative at low anorthite contents around 800 K and with convex shape at high anorthite content around 1200 K. Care should be taken not to put too much faith in the details of these results, as uncertainties can not be estimated. Yet, overall comparison with the mixing enthalpy of Carpenter (1992, assuming temperature-independent values) is striking in that negative values are predicted but with less asymmetry.

4.3 Estimating configurational entropy

Kerrick and Darken (1975) provided a simple frame to estimate configurational entropy changes ($\Delta S_{\mathrm{config}}$) in plagioclase feldspars, via estimation of the number of sites available for cation exchange. In fully disordered (randomly distributed) albite and anorthite, 4 sites

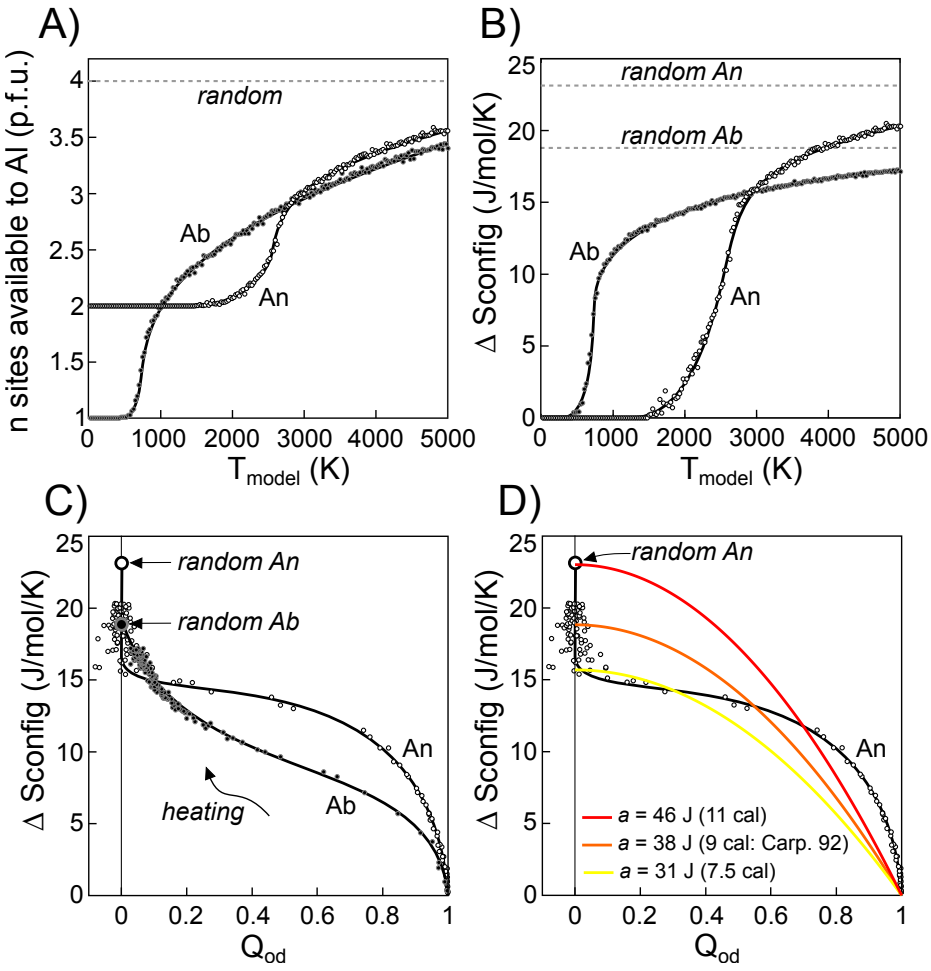

Fig. 8 Increasing randomness of $C\bar{1}$ albite and $P\bar{1}$ anorthite during heating. A) Average number of T sites effectively available to Al, a proxy to the the number of degrees of freedom of the system, p.f.u. B) Corresponding ΔS_{config} increase. C) ΔS_{config} versus macroscopic ordering. Values for fully disordered albite and anorthite are labelled as random. D) Comparison with ΔS_{config} calculated with the Landau equations and different values for the a parameter for anorthite. Carp. 92 is for Carpenter (1992). Dark bold curves are moving averages of the calculations shown as circles.

p.f.u. are accessible to Al (noted $n_{\text{acc}}^{\text{Al}} = 4$). Kerrick and Darken (1975) estimate ΔS_{config} through the number of accessible configurations Ω:

$$\Delta S_{\text{config}} = k_B \ln(\Omega) = k_B \ln\left(\frac{n_{\text{acc}}^{\text{Al}}!}{n_{\text{Al}}!(n_{\text{acc}}^{\text{Al}} - n_{\text{Al}})!}\right). \quad (2)$$

Using Stirling's approximation for factorials of large numbers, Kerrick and Darken (1975) obtained $\Delta S_{\text{config}} = 18.7$ J/mol/K between ordered and totally disordered albite, in agreement with previous estimations. The same approach yields $\Delta S_{\text{config}} = 23.1$ J/mol/K between ordered and totally disordered anorthite ($n_{\text{Al}} = 2$ p.f.u.). This is an unrealistic maximum value for geological applications as short-range ordering in anorthite remains important up

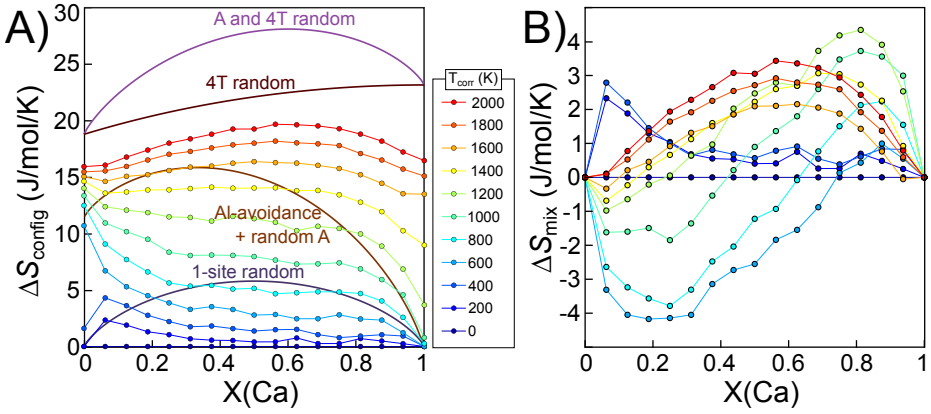

Fig. 9 A) ΔS_{config} increase estimated along the $C\bar{1}$ albite-anorthite solid solution every 200°C. Temperatures are corrected as for Fig. 7. Plain lines show values for random mixing over 1 site (such as the A site), over the four T sites, over the A site plus the four T sites, and for the Al-avoidance model with random A-site mixing of Kerrick and Darken (1975). B) Corresponding entropy of mixing. All values p.f.u.

to temperatures above its melting point. Following the reasoning of Kerrick and Darken (1975) who note that *in essence, exclusion of Al-O-Al bonds decreases the randomness of structure*, it is observed that at low temperature, Al in ordered anorthite cannot migrate because creating Al-O-Al bonds is too energetically costly (therefore $n_{\text{acc}}^{\text{Al}} = n_{\text{Al}}$ and $\Omega = 1$). The probability of any Si-Al exchange taking place is zero.

Due to the temperature-dependent short-range order found at low Q_{od} values, one cannot use the approach of Malcherek et al. (1999) to link directly $\ln(\Omega)$ to Q_{od}. Instead, the number of sites available to Al increases with temperature and ΔS_{config} was approximated by averaging the rates of Si-Al exchange in simulations, in a simplified version of thermodynamic integration. The number of sites available to Al becomes:

$$n_{\text{acc}}^{\text{Al}} = n_{\text{Al}} + \frac{n_{\text{Si-O-Al}} P_{\text{Si}\leftrightarrow\text{Al}}}{n_{\text{Al}}} \tag{3}$$

with $P_{\text{Si}\leftrightarrow\text{Al}}$ the probability of Si-Al exchange, calculated from the average acceptance rate (over the same number of tried exchanges as for Fig. 7). The number of Si-O-Al bonds $n_{\text{Si-O-Al}}$ is tied to that of Al-O-Al and Si-O-Si bonds through the relation $n_{\text{Si-O-Si}} = 4 + n_{\text{Al-O-Al}} - 4 \times X_{\text{Ca}}$, which holds for any configuration of albite, anorthite and their solid solution. ΔS_{config} is obtained from Eq. 2 and 3 using Stirling's approximation.

Albite and anorthite Figure 8 shows the estimated number of sites available to Al and the corresponding ΔS_{config} increase from the ordered configuration for albite and anorthite.

In ordered anorthite, none of the Si sites are available to Al at low temperature ($P_{\text{Si}\leftrightarrow\text{Al}} = 0$). With increasing temperature, disorder increases through increasing $P_{\text{Si}\leftrightarrow\text{Al}}$ but decreasing $n_{\text{Si-O-Al}}$ as Al-O-Al and Si-O-Si bonds appear.

In albite, disordering takes place at lower temperature because the availability of Si sites to Al is controlled by weaker second-neighbour interactions, without creating costly Al-O-Al bonds.

For both minerals ΔS_{config} increases rapidly with macroscopic disordering (Fig. 8C). For $Q_{od} = 0.75$, ΔS_{config} has reached $\sim 40\%$ of its maximum value in albite and $\sim 50\%$ in

anorthite. Above T_c and closer to $Q_{od} = 0$, ΔS_{config} keeps increasing with temperature but at slower pace. Maximum values for ΔS_{config} are not reached in the simulations, as for the number of Al-O-Al bonds not reaching random distributions (Fig. 7A). Again this reflects the importance of short-range order above T_c ($\sigma > 0$, Fig. 10A).

Figure 8D shows ΔS_{config} calculated with the Landau equations and the parametrisation of Carpenter (1992, orange curve with $a = 38$ J, identical equation for a first-order or tricritical phase transition). While absolute values are fundamentally similar to estimates of ΔS_{config} from the simulations, the latter grow initially faster with disordering than predicted by Landau theory, and the model of Carpenter (1992) predicts higher ΔS_{config} close to T_c. A value of $a \simeq 31$ J gives a better fit to the simulations just above T_c, $a \simeq 46$ J is necessary to reproduce ΔS_{config} obtained for complete disorder, but gives a much poorer fit to the data without increasing significantly the quality of the fit to nearly-ordered minerals. The sigmoid dependency of ΔS_{config} on Q_{od} found for albite cannot be reproduced with the Landau formalism where ΔS_{config} varies with Q_{od}^2.

The $C\bar{1}$ solid solution For the albite-anorthite solid solution, the low value for J_{Na-Ca} is consistent with random mixing for Na-Ca but Ca-Si interactions are relatively unfavourable (Fig. 3), implying that all A sites are not effectively available to Ca. The expression for Ω becomes:

$$\Omega = \frac{n_{acc}^{Ca}!}{n_{Ca}!(n_{acc}^{Ca} - n_{Ca})!} \cdot \frac{n_{acc}^{Al}!}{n_{Al}!(n_{acc}^{Al} - n_{Al})!} \tag{4}$$

and associated exchange probabilities $P_{Na\leftrightarrow Ca}$ and $P_{Si\leftrightarrow Al}$ are estimated from the success rates of exchange.

Figure 9A shows the obtained temperature-composition evolution of ΔS_{config} along the $C\bar{1}$ albite-anorthite solid solution, compared to the Al-avoidance model of Kerrick and Darken (1975) and to random mixing models (over the A site, the four T sites, and over the A site plus the four T sites). Overall, ΔS_{config} appears dominated by contributions from the T sites. The corresponding mixing entropy ΔS_{mix} is shown in Fig. 9B.

Consistent with the greater critical temperature of anorthite compared to albite, ΔS_{config} generally decreases with increasing anorthite content, especially between 600 and 1600 K, with a plateau between $X_{Ca} = 0.3$ and $X_{Ca} = 0.8$. Below 600 K, there is a small increase of ΔS_{config} at low anorthite content compared to albite, attributed to the greater degree of freedom of the system, where Al content remains sufficiently low for easy migration without creating Al-O-Al bonds (see Fig. 7 A). Above 1600 K, the sharp increase in ΔS_{config} of anorthite has been reached and the composition evolution of ΔS_{config} is slightly convex with maximum values around $X_{Ca} = 0.6$, far from reaching random mixing values. The Al-avoidance model of Kerrick and Darken (1975) shown for comparison uses ordered anorthite and disordered albite for end-members. In this model only two T sites are accessible to Al-Si mixing. Simulation results clearly depart from all ideal mixing models.

The evolution of ΔS_{config} translates as a positive mixing entropy (ΔS_{mix} in Fig. 9B) below $\sim$500 K, becoming strongly negative at low anorthite content around 600 K as disordering increases much faster in albite than in anorthite. For the same reason, mixing entropy appears strongly asymmetric below $\sim$1400 K.

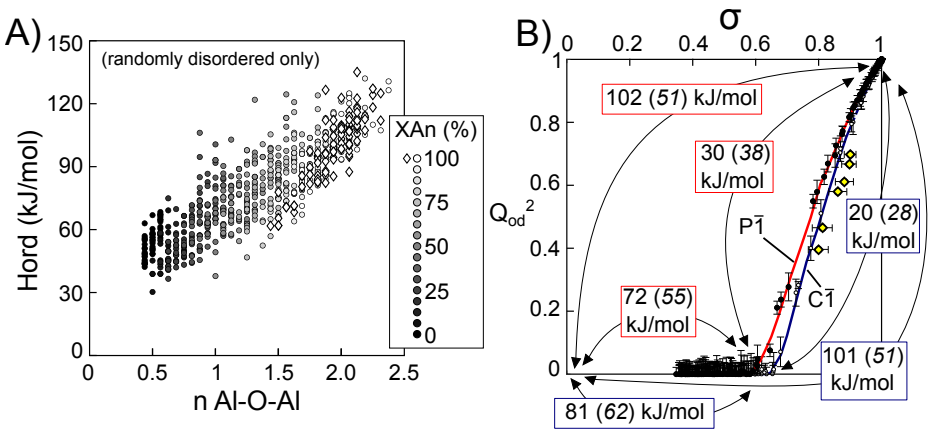

Fig. 10 Calculated ordering enthalpies. A) Enthalpy difference between structures considered as ordered and fully disordered, versus the number of Al-O-Al bonds in the disordered structure. Enthalpies are computed with GULP. The energy level of ordered structures along the $C\bar{1}$ solid solution is taken from the lowest estimated with the J_s (at T = 0 K in Fig. 7). Diamonds show results for $P\bar{1}$ anorthite. Note that the spread is large. B) Estimated enthalpy variations during disordering of $C\bar{1}$ (blue) and $P\bar{1}$ (red) anorthite. Enthalpy variations are given from ordered anorthite ($Q_{od} = 1$, $\sigma = 1$) to disordered anorthite ($Q_{od} = 0$) with or without remaining short-range order ($\sigma \sim 0.7$ and $\sigma = 0$, respectively). The first value indicates the enthalpy variation, the second value (bracketed, italics) is normalized to the number of Al-O-Al bonds. The uncertainty over the total disordering enthalpy is estimated from the standard deviation in A) at $\sim$ 10 kJ/mol.

5 Implications and discussion

5.1 Enthalpy: implications of competing short- and long-range interactions

Competition between first and second-neighbour interactions is known to be of importance for disordering in plagioclase (e.g. Vinograd and Putnis, 2001). Here second-neighbour $J_{\mathrm{Al-Al}}$ values are overall around 0.1 eV (per pair, Fig. 3, ~9.6 kJ per mole of pairs), much smaller than first-neighbour $J_{\mathrm{Al-Al}}$ values around 0.9 eV (per pair), consistent with previous studies, but as second neighbours are in greater numbers than first neighbours, competition is direct.

This implies a very strong decrease in the energetic penalty of disordering in (ordered) anorthite, as diffusive exchange of Si-Al neighbours creates three Al-O-Al bonds ($\sim +2.7$ eV for the structure) but decreases the number of second-neighbours Al-Al by ten (~ -1 eV). Slow increase of Al-O-Al bonds with temperature, and faster decrease of second-neighbour pairs (Fig. 4AB), reflect that this competition is maintained with increasing disordering, leading to the appearance of micro-domains (Fig. 5). This effect is comparatively even stronger in anorthite-rich plagioclase. Assuming an ordered, anorthite-rich plagioclase containing one Na and one Si cation in neighbouring A and T sites (keeping charge imbalance to a minimum), Si-Al exchange in the vicinity of this albitic component is greatly favoured. Any Si-Al exchange around the Si-rich T site will create two Al-O-Al bonds ($\sim +1.8$ eV) and decrease the number of second-neighbours Al-Al by nine (~ -0.9 eV), halving the energetic cost of disordering. This effect favours the presence of diffuse albite components in anorthite-rich plagioclase rather than strict exsolution features (albite-like and anorthite-like domains separated by well-defined walls), which would result in higher energies: higher number of second-neighbour Al-Al pairs (from the anorthite component),

as well as Al-O-Al bonds through domain walls due to the mutually incompatible ordering patterns of albite and anorthite. This interpretation is consistent with the analysis of Jin and Xu (2017) reporting smooth chemical variations through structural variations resembling alternating $I\bar{1}$-like lamellae in incommensurate An_{51} '*e*'-plagioclase, but comparison with the present simulations remains limited as structural variations are neglected with the J_s method.

Short-range order remains high in macroscopically-disordered plagioclase feldspars over the temperature range of the lithosphere, as seen through the number of Al-O-Al bonds being significantly less than expected for random distribution in disordered anorthite (Fig. 4), albite (Fig. 6) and their solid solution (Fig. 7).

High short-range order in macroscopically-disordered anorthite (Fig. 10 B: $\sigma \neq Q_{od}^2$) decreases ordering enthalpies from a $\sim$ 102 ($\pm$10) kJ/mol difference between ordered and randomly disordered anorthite ($\sigma = Q_{od}^2 = 0$) to a $\sim$ 30 kJ/mol ordering enthalpy – with disordered anorthite at $\sigma \approx 0.7$ for $Q_{od} = 0$. The $\pm$10 kJ/mol uncertainty is the standard deviation of the energy of structures considered as disordered here (when the number of Al-O-Al bonds was within 30% of the random value, see Fig. 10 A, calculated with GULP and used in Fig. 2).

This $\sim$ 30 kJ/mol ordering enthalpy is in agreement with the experimental results of Carpenter (1991) yielding 27 ($\pm$8) kJ/mol for the structural change between $Q_{od} = 1$ and $Q_{od} = 0$. Using these value and their NMR measurements, Phillips et al. (1992) found 39 ($\pm$12) kJ per mole of Al-Si exchange via the reaction:

$$2(\mathrm{Si}-\mathrm{O}-\mathrm{Al}) = (\mathrm{Si}-\mathrm{O}-\mathrm{Si}) + (\mathrm{Al}-\mathrm{O}-\mathrm{Al}). \quad (5)$$

Malcherek et al. (1999) obtained 40 kJ per mole of Al-Si exchange using simulations. The present modelling is consistent with $\sim$ 38 kJ per mole of Al-Si exchange.

Ordered micro-domains co-existing with anti-phase domains (as in Fig. 5) allow reaching macroscopic disorder with a minimum number of Al-Al linkages. It is noteworthy that the transition from ordered anorthite to $\sigma \approx 0.7$ and $Q_{od} = 0$ represents only a third of the total ordering enthalpy (Fig. 10). Increasing disordering above T_c is more energetically costly ($\sim$ 72 kJ/mol from $\sigma \approx 0.7$ to $\sigma = 0$, representing $\sim$ 55 kJ per mole of Al-Si exchange) as the beneficial effect of second-neighbour interactions disappears with increasing randomness.

In albite and albitic plagioclase, complete disordering is much less costly (Fig. 10 A) than in anorthite ($\sim$ 30 kJ/mol instead of $\sim$ 102 kJ/mol). This mainly reflects the effect of composition where Al-Al linkages are less likely at lower Al content (see also Dove et al., 1996; Vinograd et al., 2001). However because disordering to $Q_{od} = 0$ initially takes place with very little creation of Al-Al linkages (Fig. 6 and 7), it is not meaningful to express ordering enthalpies per mole of Al-O-Al bonds as the energetic cost arises from second-neighbour interactions. In other words, reaction 5 remains an important control to Si-Al exchange in that it is avoided during disordering, but for the same reason this reaction does not reproduce disordering in albitic plagioclase over lithospheric temperatures.

5.2 Effect over configurational entropy

Configurational entropy exerts a fundamental control over the thermodynamics of mixing and ordering reactions.

In the simulations, accepting a single cation exchange leads to negligible contribution of $\Delta S_{\mathrm{config}}$ to the energetic increase ($\sim$0.003 eV at 25 K to $\sim$0.02 eV at 5000 K, much smaller than enthalpy contributions from the J_s), therefore enthalpy variations control cation

exchange. The contribution of ΔS_{config} to the chemical potential becomes significant as soon as macroscopic disorder increases (Fig. 8). If ordered albite and anorthite are selected as thermodynamic components, the contribution of ΔS_{config} to the chemical potential appears to be of the same magnitude or greater than that of ordering enthalpy ($T \times \Delta S \geq$ Hord). Consequently activity-composition relations in plagioclase feldspars are at least as much affected by entropy as by enthalpy changes during disordering.

The contribution of ΔS_{config} is important at low anorthite content from temperatures as low as 200 K but remains small for anorthite up to $\sim$1000 K (Fig. 8 and 9). Unfortunately, none of the simple mixing models usually cited in the literature, such as random Si-Al mixing over 2 or 4 sites, with or without Al avoidance, appear to draw a realistic picture of cation distribution over an extended composition range (Fig. 9) due to the complexity of competing first- and second-neighbour interactions (Fig. 7 A and C for example). Appearance of micro-domains at high anorthite content during disordering (e.g. Fig. 5) is inconsistent with distributing Al into fixed preferred sites. In addition, an ordered "low albite" end-member appears acceptable for low temperatures (Qod > 0.9) but the "high albite" end-member contains short-range order that cannot be well represented by any model where mixing is not temperature-dependent, because average site distributions are temperature-dependent (Fig. 6D) and do not reach random mixing values.

Therefore using non-ideal mixing models is necessary, and large mixing parameters may be expected. The magnitude of the values obtained here for ΔS_{config} and mixing entropy (Fig. 8 and 9) remain speculative considering that uncertainties from the modelling are very poorly constrained, particularly over temperature. However, the asymmetry of the mixing entropy and its temperature variations are logical consequences of the large temperature difference between disordering of albite and anorthite. Benisek et al. (2010) suggested that 'the asymmetry of the excess mixing properties may change with temperature', which is clearly reflected by this study.

Examples of asymmetric and/or negative mixing entropy in silicate solid solutions are plentiful, such as for the Mg-Fe exchange in orthopyroxene (Berman and Aranovich, 1996), the muscovite-paragonite solvus in mica (Chatterjee and Flux, 1986), the clinochlore-sudoite solvus in chlorite (Vidal et al., 2006), the diopside-hedenbergite solution in omphacite (Meyre et al., 1997) and even in the regression of Benisek et al. (2004) for the albite-anorthite solution (considered continuous). But the strong temperature dependency of ΔS_{config} – hence that of the mixing entropy – is a challenge that classical formalisms with Margules parameters (see e.g. Berman, 1988) cannot meet without allowing W_S terms to vary with temperature. In the temperature range of stability of the $C\bar{1}$ solid solution (approximated to 600 - 1600 K for comparison with Fig. 9B), the present results suggest $W_{S\text{Ab}-\text{An}} \simeq -37$ and $W_{S\text{An}-\text{Ab}} \simeq -58$ at 600 K, $W_{S\text{Ab}-\text{An}} \simeq -8$ and $W_{S\text{An}-\text{Ab}} \simeq -53$ at 1100 K, and with a much poorer fit $W_{S\text{Ab}-\text{An}} \simeq W_{S\text{An}-\text{Ab}} \simeq -30$ at 1600 K (W_S in J/mol/K). These values are obtained using ideal contributions from the Al-avoidance model of Kerrick and Darken (1975), showing much more pronounced curvature for ΔS_{config} than the current simulation results (Fig. 9A). If ideal contributions of the albite and anorthite components to mixing entropy are taken as equal to their mole fraction, the following values are obtained: $W_{S\text{Ab}-\text{An}} \simeq -15$ and $W_{S\text{An}-\text{Ab}} \simeq -51$ at 600 K, $W_{S\text{Ab}-\text{An}} \simeq 11$ and $W_{S\text{An}-\text{Ab}} \simeq -42$ at 1100 K, and $W_{S\text{Ab}-\text{An}} \simeq W_{S\text{An}-\text{Ab}} \simeq -20$ at 1600 K.

For anorthite, differences from the parametrisation by Carpenter (1992, Fig. 8D) are small but highlight difficulties in defining Q_{od} for meaningful comparison between simulations and diffraction experiments. At face value, results of the simulations suggest weaknesses of the Landau equations in reproducing disordering with temperature-independent parameters, and a possible overestimation of the a parameter by Carpenter (1992). It is also

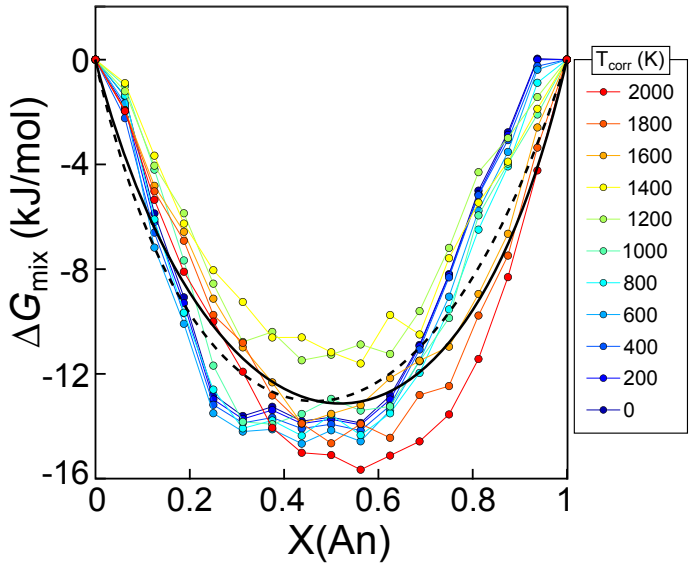

Fig. 11 Gibbs free energy of mixing estimated from mixing enthalpy and entropy (Fig. 7F and 9) along the $C\bar{1}$ solid solution. The dashed dark curve is calculated at 1073 K with $W_{GAbAn} = -20$ kJ/mol and $W_{GAnAb} = -35$ kJ/mol using mole fractions of the albite and anorthite components for ideal contributions. The bold dark curve is also calculated at 1073 K but with the Kerrick and Darken (1975) Al-avoidance model for ideal contributions, and $W_{GAb-An} = -10$ kJ/mol and $W_{GAn-Ab} = -15$ kJ/mol.

noteworthy that the algorithm only allowing for nearest-neighbour cation swaps may be restrictive for evaluating ΔS_{config} (and Q_{od}), for example if longer jumps take place. Yet, as for enthalpy, at first order the present estimates of ΔS_{config} are consistent with the results of Carpenter (1992).

5.3 Implications for mixing and activity-composition relations

The large values for ordering enthalpy of anorthite obtained here (Fig. 10), together with the large negative mixing enthalpy along the $C\bar{1}$ solid solution (Fig. 7 F) are in much better agreement with the results of Carpenter (1992, and references therein) than with the modelling based on near-ideal Si-Al mixing and small ordering enthalpies of Holland and Powell (1992) and Holland and Powell (2003) fitted to phase equilibria.

Estimated mixing enthalpy (Fig. 7F) and ΔS_{config} variations (Fig. 8A) yield the Gibbs mixing energy (ΔG_{mix}) shown in Fig. 11. The combined effects of negative mixing enthalpy and large ΔS_{config} lead to negative ΔG_{mix} values. The temperature dependency is weak and possibly not meaningful considering the probably large uncertainties at this point Using the Al-avoidance model of Kerrick and Darken (1975) for ideal activities, Margules parameters of $W_{GAb-An} = -10$ kJ/mol and $W_{GAn-Ab} = -15$ kJ/mol give an approximate fit to ΔG_{mix} at 800°C (bold curve on Fig. 11). Assuming that ideal contributions of the albite and anorthite components are equal to their mole fraction, Margules parameters of approximately $W_{GAb-An} = -20$ kJ/mol and $W_{GAn-Ab} = -35$ kJ/mol give an equally good fit (dashed curve on Fig. 11). It is noteworthy that only one pair of W parameters is needed, even though mixing takes place on two sites (see Powell and Holland, 1993).

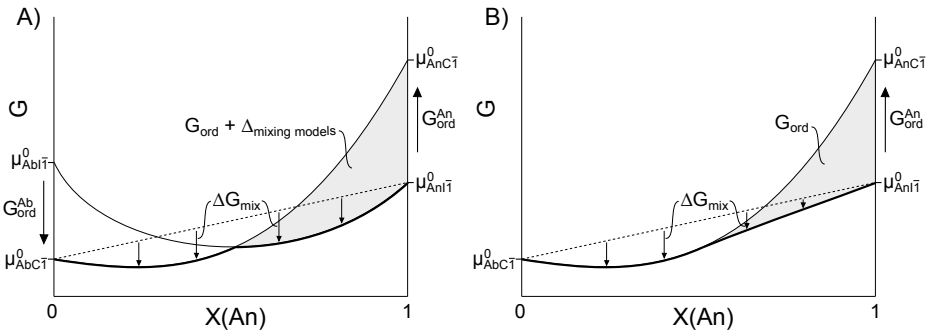

Fig. 12 Modelling approaches, using (A) four end-members and two distinct solid solution models or (B) only one solid solution, to which G_{ord} is added from Landau equations. The chemical potentials of the end-members are noted μ^0. ΔG_{mix} is the difference between the Gibbs energy of the stable mixture and the combination of the equilibrium end-members (here, $Ab^{C\bar{1}}$ and $An^{I\bar{1}}$). The other end-members are metastable.

The magnitude and shape of ΔG_{mix} derived here are consistent with that of the model of Carpenter (1992). The ordering energy G_{ord} calculated with the Landau equations (see e.g. Carpenter and McConnell, 1984) must be added to the mixing model along the albite-anorthite solid solution. There are essentially two approaches: using a mixing model for each domain and four end-members, or a mixing model in the $C\bar{1}$ domain only, requiring only three end-members. Figure 12 shows the corresponding shapes of ΔG_{mix}. The difference between the $C\bar{1}$ and $I\bar{1}$ anorthite end-members is the same in both models, and equals the ordering energy of anorthite. The Gibbs energy of the mixture is that of the lowest domain (bold curve on Fig. 12) and ΔG_{mix} is shown as the difference between the combination of the chemical potential of the stable end-members (dashed line) and the energy of the mixture. A crucial point is that the activity of the end-members in the stable phase depends on the ordering energy and on the mixing model, such as, for the three end-member case (Fig. 12B):

$$\mathrm{R}T\ln a_{\mathrm{Ab,C\bar{1}}} = \mathrm{R}T\ln X_{\mathrm{Ab}} + \mathrm{R}T\ln\gamma^{\mathrm{W}}_{\mathrm{Ab,C\bar{1}}} + \mathrm{R}T\ln\gamma^{\mathrm{ord}}_{\mathrm{Ab}} \tag{6}$$

$$\mathrm{R}T\ln a_{\mathrm{An,C\bar{1}}} = \mathrm{R}T\ln X_{\mathrm{An}} + \mathrm{R}T\ln\gamma^{\mathrm{W}}_{\mathrm{An,C\bar{1}}} + \mathrm{R}T\ln\gamma^{\mathrm{ord}}_{\mathrm{An}} \tag{7}$$

$$\mathrm{R}T\ln a_{\mathrm{An,I\bar{1}}} = \mathrm{R}T\ln X_{\mathrm{An}} + \mathrm{R}T\ln\gamma^{\mathrm{W}}_{\mathrm{An,C\bar{1}}} + \mathrm{R}T\ln\gamma^{\mathrm{ord}}_{\mathrm{An}} - G^{\mathrm{An}}_{\mathrm{ord}} \tag{8}$$

where γ^{W} is an activity coefficient arising from non-ideality as classically modelled with Margules or ASF parameters (see Holland and Powell, 1992, for the formalism). The term $G^{\mathrm{An}}_{\mathrm{ord}}$ allows activity to be referred to the equilibrium end-member in the $I\bar{1}$ domain. $\mathrm{R}T\ln\gamma^{\mathrm{ord}}$ is the deviation from ideality arising from ordering in the $I\bar{1}$ domain:

$$\mathrm{R}T\ln\gamma^{\mathrm{ord}}_{\mathrm{An}} = G_{\mathrm{ord}} + (1 - X_{\mathrm{An}})\frac{\partial G_{\mathrm{ord}}}{\partial X_{\mathrm{An}}} \tag{9}$$

$$\mathrm{R}T\ln\gamma^{\mathrm{ord}}_{\mathrm{Ab}} = G_{\mathrm{ord}} - X_{\mathrm{An}}\frac{\partial G_{\mathrm{ord}}}{\partial X_{\mathrm{An}}} \tag{10}$$

and $\mathrm{R}T\ln\gamma^{\mathrm{ord}} = 0$ in the $C\bar{1}$ domain. It is noteworthy that in the $I\bar{1}$ domain, the chemical potential of the $I\bar{1}$ anorthite component is lower (more negative) than that of the $C\bar{1}$ anorthite component (in anorthite: $\mu^0_{\mathrm{An}I\bar{1}} < \mu^0_{\mathrm{An}C\bar{1}}$, Fig. 12). To describe $\mu_{\mathrm{An}C\bar{1}}$ in $I\bar{1}$ anorthite, equating

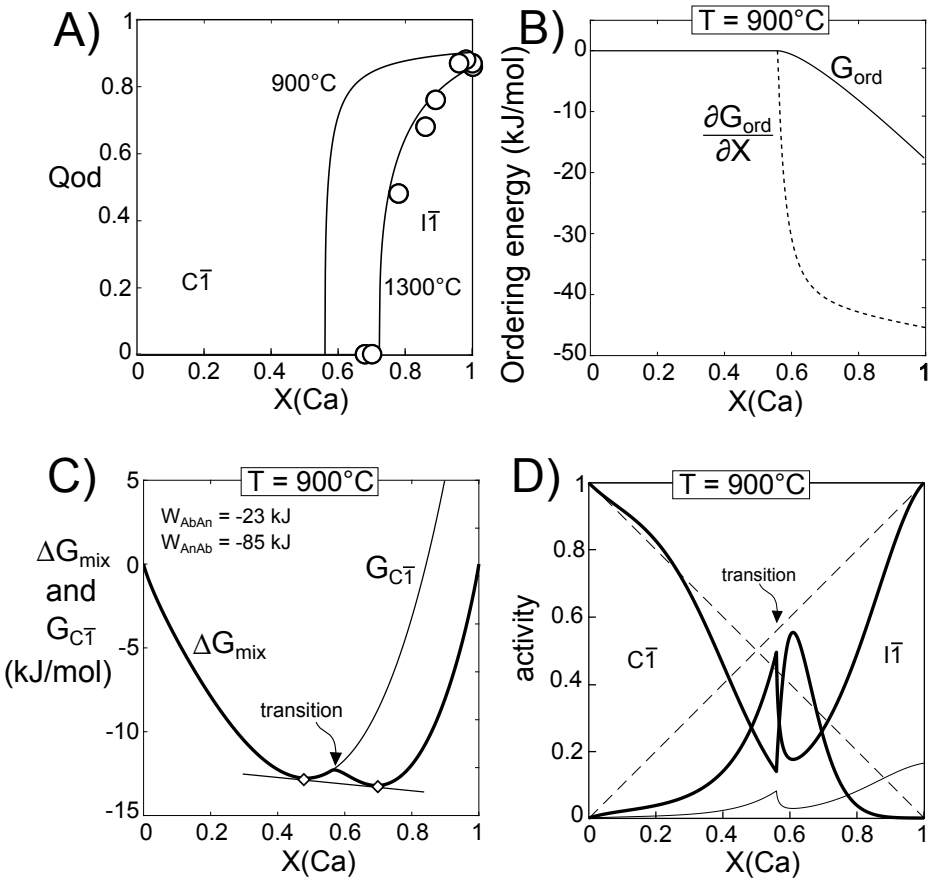

Fig. 13 Ordering and mixing energetics calculated using a generalised version of the parametrization of Carpenter (1992), where the $C\bar{1} \rightleftharpoons I\bar{1}$ transition is first-order for anorthite but tricritical along the albite-anorthite solid solution. A) Q_{od} calculated at 900 and 1300 °C, compared to the 1300°C measurements of (Angel et al., 1990, open circles) . B) Ordering energy from Landau equations (plain curve) and its derivative (dashed) at 900°C. C) ΔG_{mix} (bold curve) and metastable extension of the $C\bar{1}$ end-members in the $I\bar{1}$ domain (thin curve, compare with 12A). D) Obtained activity-composition relation. Straight dashed lines show activity = composition. Bold curves are for the stable end-members ($Ab^{C\bar{1}}$ and $An^{I\bar{1}}$), thin curve for the virtual end-member ($An^{C\bar{1}}$). Random mixing over the 4 T sites and the Na-Ca site has been used for ideal activities.

chemical potentials yields: $\mu_{AnC\bar{1}} = \mu^0_{AnC\bar{1}} + RT\ln\gamma^{ord}_{An} = \mu^0_{AnI\bar{1}}$. It follows that $RT\ln\gamma^{ord}_{An}$ is negative and therefore the activity of the $C\bar{1}$ anorthite component is below 1 when $I\bar{1}$ anorthite is stable ($a_{An,I\bar{1}} = 1$). This may appear trivial but is a source of confusion (compare e.g. Carpenter and McConnell (1984) Fig. 5 and Carpenter and Ferry (1984) Fig. 2).

From there, proposing a robust thermodynamic model for structural changes and phase equilibria relies on correct parametrization of the mixing parameters (Margules or ASF parameters) and of the Landau parameters (a, b, and c with a first-order model, see solutions given in Carpenter, 1988). The latter proved very difficult, as Landau parameters may vary with X_{Ca}, strongly affecting activity coefficients in particular (through Eq. 9 and 10). In

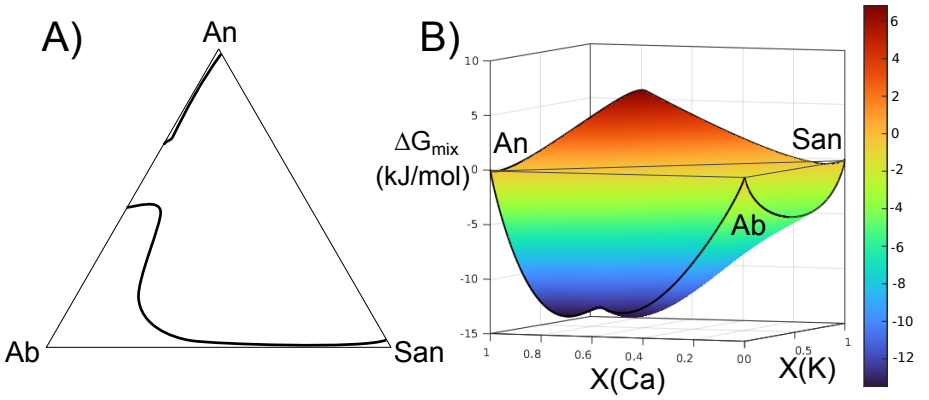

Fig. 14 Illustrative phase diagram for ternary feldspars (albite-anorthite-sanidine) obtained with the Landau equations in the $I\bar{1}$ domain and a non-ideal mixing model at 900°C (as for Fig. 12B and 13). A) Stable domains, B) Three-dimensional view of ΔG_{mix}. The unintentional solvus between albite and anorthite also causes a large difference in the K content of the albite-rich and the anorthite-rich phases. The anorthite-sanidine binary is largely unstable due to to the combined effects of the Landau equations and moderate $W_{\mathrm{An-San}}$.

addition, T_c also varies with X_{Ca}, apparently linearly in the range 800-1400°C, further complicating the expression of $\frac{\partial G_{\mathrm{ord}}}{\partial X_{\mathrm{An}}}$.

Carpenter (1992) studied the parametrization of Landau coefficients along the albite-anorthite solid solution at 1300°C, crossing the $C\bar{1} \rightleftharpoons I\bar{1}$ transition around $X_{\mathrm{Ca}} = 0.78$. In their favoured model, the a parameter is constant at the value of anorthite and the values of b and c change linearly with composition, with $b = 0$ close to the transition. In this view there is a tricritical point at $X_{\mathrm{Ca}} = 0.78$ and the transition is second-order ($b > 0$) at lower anorthite content. Unfortunately, this approach does not apply well to lower temperatures (transition below $X_{\mathrm{Ca}} = 0.78$), first because Landau equations imply that $c = a.T_c$ if the transition is tricritical, and that c vanishes (or is negligible) if the transition is second-order. Attempts to, for example, zero the c parameter in the second-order domain may yield a satisfying expression for G_{ord} but its derivative will show a discontinuity bringing chaos to activity coefficients (Eq. 9 and 10), and c cannot be or approach zero at the phase transition (otherwise $\mathrm{Q_{od}} \rightarrow \infty$). Forcing the b parameter to zero value at the phase transition is also unsatisfactory, as this implies that b varies with temperature, which is at odds with Landau theory. The phase transition should be described of the same order along the albite-anorthite solid solution to allow smooth activity coefficient variations.

For anorthite, Carpenter (1992) showed that the first-order model gives the best fit to experimental constraints over $\mathrm{Q_{od}}$, linearly extrapolating T_c to 2010°C. The transition being thermodynamically continuous along the albite-anorthite solid solution, a tricritical model ($b = 0$) is probably better than a first-order model (see also Redfern and Salje, 1987; Salje, 1987), but a tricritical model implies increasing T_c to $\sim$ 3250°C to reach the same quality of fit to the measured ordering degree of anorthite as for the first-order model. In turn, this implies that the temperature of the phase transition increases very non-linearly above $\sim \mathrm{An_{78}}$, with strong implications for γ^{ord} (Eq. 9 and 10).

Figure 13 illustrates calculations using the least problematic model, where the phase transition is first-order for anorthite and tricritical along its solid solution with albite ($b = 0$ and $c = a.T_c$ at the phase transition, even though this implies temperature-dependent Landau

parameters). Strikingly, a wide solvus appears around the phase transition, despite strongly negative Margules parameters based on the mixing enthalpy of Carpenter (1992) and the mixing entropy of Benisek et al. (2010). The values are only illustrative and should not be directly used for petrological applications.

Compositional continuity along the albite-anorthite solid solution is suggested by available data above at least 900°C, and definitive evidence for a solvus above the 'e_1' field of plagioclase is still missing. A limited miscibility gap has been suggested around the $C\bar{1} \rightleftharpoons I\bar{1}$ transition near 800°C (e.g., McConnell, 1974; Jin et al., 2021) but remains uncertain. In any case, negative Margules parameters in the $C\bar{1}$ domain are implied, as in Carpenter (1992), and smooth variations of ΔG_{mix} around the phase transition. In particular, the second derivative of ΔG_{mix} with respect to X_{An} must remain positive to avoid apparition of a solvus. However, the form of the equation governing G_{ord} implies G_{ord} becomes very rapidly more negative with increasing X_{Ca}, inevitably leading to a solvus around the transition (however small) and to strong variations in γ^{ord}. The unwanted presence of a solvus generated by the Landau approach has already been mentioned (e.g., Carpenter, 1992), leading Holland and Powell (1992) to dismiss their Landau model.

Smoothly-evolving activity coefficients appear necessary, and Carpenter and Ferry (1984) mention the difficulty of deriving activity coefficients close to the transition. Interestingly, the fluid-plagioclase exchange data of Orville (1972) and Schliestedt and Johannes (1990) suggest smooth and near-ideal activity-composition relations in the range 600-700°C (see fits obtained by Holland et al., 2022), without discontinuity for activity coefficients in pressure-temperature-composition domains containing phase transitions and solvi. Holland et al. (2022) state that phase transitions and the presence of 'e' plagioclase "appear to have only small consequences for the thermodynamics of the solid solution", but Schliestedt and Johannes (1990) highlight that their experiments did not allow equilibration of Al-Si distribution, yielding disordered plagioclase only. Therefore drawing conclusions about the relative impacts of phase transitions and of cation exchange over activity-composition relations for the entire albite-anorthite solid solution requires additional work and will probably remain difficult. Previous work, e.g. on sodium feldspar including the $C\bar{1} \rightleftharpoons C2/m$ transition (Salje, 1985; Salje et al., 1985), has shown that the structural parameter (Q, the "displacive driving force") is dominant over Al-Si ordering ($\mathrm{Q_{od}}$) in high albite, and inversely in low albite.

Extrapolation of the approach to ternary feldspars is straightforward in terms of formalism, but again requires better parametrisation. An example is shown in Fig. 14, assuming identical Landau coefficients for the sanidine-anorthite binary as for albite-anorthite, and $W_{\mathrm{San-An}} = 20$ kJ. Random mixing over the 4 T sites and the A site has been used for ideal activities. The mixing model for albite-sanidine equilibria is described in Appendix A.

The main differences between the models of Holland et al. (2022), Benisek et al. (2010) and the formalism using Landau equations (this study) are the undesired albite-anorthite solvus and the K content of plagioclase around the phase transition.

6 Conclusion

The results of atomistic modelling using Monte-Carlo simulations argue in favour of large ordering enthalpies and entropies for anorthite, as well as for very significant short-range ordering maintained in macroscopically-disordered structures ($\mathrm{Q_{od}} = 0$) keeping the number of Al neighbours to a minimum, in agreement with previous studies (Phillips et al., 1992, among others). In the $C\bar{1}$ domain, large and asymmetrical mixing enthalpy and entropy along the albite-anorthite solid solution are obtained, resulting in largely negative but mostly

symmetrical ΔG_{mix}. Competition between first- and second-neighbour interactions is key to the complexity of Al-Si ordering in plagioclase feldspars, even though these interactions may be idealised and simplistic with the J_S method.

Combining Landau theory equations in the $I\bar{1}$ domain to a non-ideal mixing model in the $C\bar{1}$ domain appears to provide reliable results in terms of energy and ordering. Unfortunately, the chosen Landau equations also appear impossible to parametrise for the albite-anorthite solid solution to yield realistic activity-composition relations and phase relations, and the atomistic modelling is too crude to provide a thermodynamic model reflecting the complexities of phase equilibria within this solid solution. On the other hand, activity models based on near-ideal mixing appear erroneous in the light of the necessary large mixing enthalpies and entropies, but have successfully modelled phase equilibria in many applications to natural rocks. It is likely that the constraints used to derive such models (e.g. in the recent model of Holland et al., 2022) do not represent the true equilibrium values, due to e.g. incomplete Al-Si order (Schliestedt and Johannes, 1990) and/or biased experimental phase equilibria (see discussion in Benisek et al., 2010). In this case, the success of near-ideal mixing models would probably be explained by overall correct symmetry of these models and absence of solvus, with the difference (Gibbs mixing energy insufficiently negative and/or solvi ignored) being minor for petrological applications to high-temperature rocks, and where modelling the equilibrium structure and stability gaps of lower-temperature plagioclase such as in the '*e*' domain may be perceived as unnecessary. Yet the analysis of Jin et al. (2021) sets the temperature above which stability gaps become significant well above 800°C, and it appears that using Landau theory would be much more satisfying to reconcile crystallographic data to phase equilibria. Overcoming apparent incompatibilities between thermodynamic formalisms is required, possibly by decoupling Al-Si order parameters from structural parameters.

Acknowledgements Aline Govin and Clément Herviou are warmly thanked for enduring years of complaining about plagioclase feldspars. Detailed reviews by Victor Vinograd and especially Ross John Angel greatly helped improving the manuscript and are gratefully acknowledged.

Table 1 Values of the selected potentials. Corresponding equations are available elsewhere (e.g., Gale, 1997).

Potential type	Atoms	Parameter values			
		A (eV)	ρ (Å)	C (eV.Å^6)	
Buckingham	Si-O$_{\mathrm{shell}}$	1283.9073	0.3205	10.6616	
(r_{max} = 12 Å)	Al-O$_{\mathrm{shell}}$	1460.3	0.29912	0	
	Ca-O$_{\mathrm{shell}}$	2272.74	0.2986	0	
	Na-O$_{\mathrm{shell}}$	5836.885	0.2387	0	
	O$_{\mathrm{shell}}$-O$_{\mathrm{shell}}$	22764	0.149	27.88	
Core-shell spring	O$_{\mathrm{core}}$-O$_{\mathrm{shell}}$	K = 74.92 eV.Å^{-2}			
		k (eV.rad^{-2})	Θ_0 (°)	r_{max} (Å) cat.-O$_{\mathrm{shell}}$	r_{max} (Å) O$_{\mathrm{shell}}$-O$_{\mathrm{shell}}$
Three-body	O$_{\mathrm{shell}}$-Si-O$_{\mathrm{shell}}$	2.0972	109.47	1.8	3.2
	O$_{\mathrm{shell}}$-Al-O$_{\mathrm{shell}}$	2.0972	109.47	1.8	3.2

Table 2 Values of the regressed interaction energies *Js* and energy constants along the $C\bar{1}$ solid solution and for $P\bar{1}$ anorthite used to produce Fig 2.

Interaction	Value (eV)	
	Ab-An ($C\bar{1}$)	An ($P\bar{1}$)
First-neighbour interactions (Al-O-Al)		
$d_{\mathrm{Al-Al}} < 3.1$ Å	$0.95 - 0.13X_{\mathrm{Ca}}$	0.81
$d_{\mathrm{Al-Al}} > 3.1$ Å	$0.87 - 0.02X_{\mathrm{Ca}}$	0.72
Second-neighbour interactions (Al-O-X-O-Al)		
T2o-T2m	0.23	0.11
T2m-T2m	0.16	-0.09
T1m-T1m	0.13	-0.06
T1o-T1m	0.13	0.16
T1o-T2o	0.12	0.06
T1m-T2m	0.11	0.14
T2o-T2o	0.10	0.21
T1m-T2o	0.06	0.05
T1o-T1o	0.06	0.05
T1o-T2m	0.03	0.04
Others		
Ca-Si	0.31	–
Ca-Na	-0.08	–
Composition-related terms		
$\Delta E0$	23.64	–
W	0.38	–

A (Appendix) Mixing model and phase equilibria along the albite-sanidine binary

Mixing parameters may be analytically derived from phase equilibria along binaries by equating chemical potentials of phase components (see derivation in De Capitani and Peters, 1982; Dubacq et al., 2013). Importantly, the phase equilibrium is independent from the standard-state chemical potentials which disappear during derivation in some cases. Along the albite-sanidine binary, there is a pressure-temperature dependent solvus with binodal compositions reported by Thompson and Waldbaum (1969) around 0.2 GPa - mostly using selected data from Orville (1963) and Luth and Tuttle (1966) - and by Goldsmith and Newton (1974) around 1.5 GPa. The mixing parameters depend on the model selected for ideal mixing, even though this is not explicitly stated by De Capitani and Peters (1982) and Dubacq et al. (2013). The following expressions allow estimating $W_{\mathrm{Ab-San}}$ and $W_{\mathrm{San-Ab}}$ with various ideal mixing models:

$$W_{\mathrm{Ab-San}} = \frac{RT}{(x_1-x_2)^3}(-2\ln(a^{\mathrm{Ab}}_{x_1})(x_1^2+x_1(x_2-2)+(x_2-1)^2)+ \\ 2\ln(a^{\mathrm{Ab}}_{x_2})(x_1^2+x_1(x_2-2)+(x_2-1)^2)+ \\ (2x_1^2+x_1(2x_2-1)+x_2(2x_2-1))(\ln(a^{\mathrm{San}}_{x_1})-\ln(a^{\mathrm{San}}_{x_2}))) \tag{11}$$

$$W_{\mathrm{San-Ab}} = \frac{RT}{(x_1-x_2)^3}(-(\ln(a^{\mathrm{Ab}}_{x_1})(2x_1^2+x_1(2x_2-5)+2x_2^2-5x_2+4))+ \\ \ln(a^{\mathrm{Ab}}_{x_2})(2x_1^2+x_1(2x_2-5)+2x_2^2-5x_2+4)+ \\ 2(x_1^2+x_1(x_2-1)+(x_2-1)x_2)(\ln(a^{\mathrm{San}}_{x_1})-\ln(a^{\mathrm{San}}_{x_2}))) \tag{12}$$

where x_1 is the K content of the A site (K/(K+Na)) of the first phase with $a^{\mathrm{Ab}}_{x_1}$ the activity of the albite component in this phase, and so on.

Figure A1 presents values obtained with the ordered model (B) and with the Al-avoidance model of Kerrick and Darken (1975) (C). For the randomly disordered 4T model, values are identical to B due to analytical simplification. Values from each model will fit the phase diagram identically, but the ordered and 4T models allow straightforward fitting of the pressure-temperature evolution of the mixing parameters (Fig. A1B). With the Al-avoidance model, mixing parameters vary strongly non-linearly, especially near the critical mixing point, as evident from Fig. A1C. The selected parametrization uses the ordered (or 4T) model and:

$$W_{\mathrm{Ab-San}} = 34.958 - 0.0278 * T + 0.0280 * P \tag{13}$$

$$W_{\mathrm{San-Ab}} = 13.847 - 0.00932 * T + 0.0536 * P \tag{14}$$

with T temperature (in K, referred to standard temperature) and P pressure (in GPa). The obtained phase diagram is shown with experimental binodal compositions in Fig. A1A.

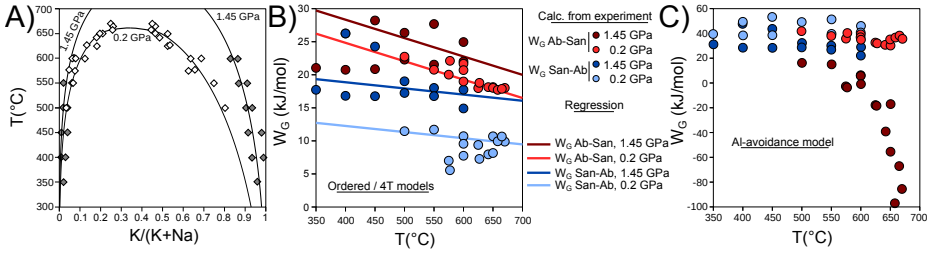

Fig. A1 Experimental phase equilibria along the albite-sanidine binary (A) and corresponding Margules parameters, using B) an ordered ideal mixing model (or a 4T-disordered model), and C) the Al-avoidance model of Kerrick and Darken (1975). Margules parameters in B) are fitted using equations 13 and 14 and shown here as lines. This regression allows calculating the curves shown in A). Experimental results are from Orville (1963), Luth and Tuttle (1966) and Goldsmith and Newton (1974).

References

Angel RJ, Carpenter MA, Finger LW (1990) Structural variation associated with compositional variation and order-disorder behavior in anorthite-rich feldspars. American Mineralogist 75(1-2):150–162, https://pubs.geoscienceworld.org/ammin/article-pdf/75/1-2/150/4217553/am75_150.pdf

Ashcroft NW, Mermin ND (1976) Solid state physics. New York: Holt and Rinehart and Winston

Benisek A, Kroll H, Cemič L (2004) New developments in two-feldspar thermometry. American Mineralogist 89(10):1496–1504, DOI 10.2138/am-2004-1018

Benisek A, Dachs E, Kroll H (2010) A ternary feldspar-mixing model based on calorimetric data: development and application. Contributions to Mineralogy and Petrology 160:327–337, DOI 10.1007/s00410-009-0480-8

Berman R (1988) Internally-consistent thermodynamic data for minerals in the system Na_2O-K_2O-CaO-MgO-FeO-Fe_2O_3-Al_2O_3-SiO_2-TiO_2-H_2O-CO_2. Journal of Petrology 29(2):445–522

Berman RG, Aranovich LY (1996) Optimized standard state and solution properties of minerals. Contributions to Mineralogy and Petrology 126:1–24, URL http://dx.doi.org/10.1007/s004100050232, 10.1007/s004100050232

Bosenick A, Dove MT, Myers ER, Palin EJ, Sainz-Diaz CI, Guiton BS, Warren MC, Craig MS, Redfern SAT (2001) Computational methods for the study of energies of cation distributions: applications to cation-ordering phase transitions and solid solutions. Mineralogical Magazine 65(2):193–219, DOI 10.1180/002646101550226

Carpenter M (1988) Physical Properties and Thermodynamic Behaviour of Minerals, Springer, Dordrecht, chap Thermochemistry of Aluminium/Silicon Ordering in Feldspar Minerals, pp 265–323. DOI 10.1007/978-94-009-2891-6{_}9

Carpenter M, Ferry J (1984) Constraints on the thermodynamic mixing properties of plagioclase feldspars. Contributions to Mineralogy and Petrology 87(2):138–148, DOI 10.1007/BF00376220

Carpenter M, McConnell J (1984) Experimental delineation of the $C1 = I1$ transformation in intermediate plagioclase feldspars. American Mineralogist 69(1-2):112–121

Carpenter MA (1991) Mechanisms and kinetics of Al-Si ordering in anorthite: II. Energetics and a Ginzburg-Landau rate law. American Mineralogist 76(7-8):1120–1133, https://pubs.geoscienceworld.org/ammin/article-pdf/76/7-8/1120/4208222/am76_1120.pdf

Carpenter MA (1992) Equilibrium thermodynamics of Al/Si ordering in anorthite. Physics and Chemistry of Minerals 19(1):1–24, DOI 10.1007/BF00206796

Carpenter MA (1994) Feldspars and their Reactions, Springer Netherlands, Dordrecht, chap Subsolidus Phase Relations of the Plagioclase Feldspar Solid Solution, pp 221–269. DOI 10.1007/978-94-011-1106-5_6, URL https://doi.org/10.1007/978-94-011-1106-5_6

Carpenter MA, McKnight REA, Howard CJ, Zhou Q, Kennedy BJ, Knight KS (2009) Characteristic length scale for strain fields around impurity cations in perovskites. Phys Rev B 80:214101, DOI 10.1103/PhysRevB.80.214101

Chatterjee ND, Flux S (1986) Thermodynamic Mixing Properties of Muscovite-Paragonite Crystalline Solutions at High Temperatures and Pressures, and their Geological Applications. Journal of Petrology 27(3):677–693, DOI 10.1093/petrology/27.3.677

De Capitani C, Peters T (1982) Corresponding states in binary solutions and graphical determination of Margules parameters. Contributions to Mineralogy and Petrology 81:48–58, DOI 10.1007/BF00371158

Dove M, Thayaparam S, Heine V, Hammonds K (1996) The phenomenon of low Al-Si ordering temperatures in aluminosilicate framework structures. American Mineralogist 81:349–362, DOI 10.2138/am-1996-3-409

Dove MT (2001) Computer simulations of solid solutions. In: Solid Solutions in Silicate and Oxide Systems, Mineralogical Society of Great Britain and Ireland, DOI 10.1180/EMU-notes.3.10, URL https://doi.org/10.1180/EMU-notes.3.10

Dubacq B, Plunder A (2018) Controls on Trace Element Distribution in Oxides and Silicates. Journal of Petrology 59(2):233–256, DOI 10.1093/petrology/egy027

Dubacq B, Vidal O, Lewin E (2011) Atomistic investigation of the pyrophyllitic substitution and implications on clay stability. American Mineralogist 96(2-3):241–249, DOI 10.2138/am.2011.3564

Dubacq B, Bickle MJ, Evans KA (2013) An activity model for phase equilibria in the H_2O-CO_2-NaCl system. Geochimica et Cosmochimica Acta 110(0):229 – 252, DOI 10.1016/j.gca.2013.02.008

Elkins LT, Grove TL (1990) Ternary feldspar experiments and thermodynamic models. American Mineralogist 75(5-6):544–559, https://pubs.geoscienceworld.org/msa/ammin/article-pdf/75/5-6/544/4217704/am75_544.pdf

Fegley B, Treiman AH, Sharpton VL (1992) Venus surface mineralogy - Observational and theoretical constraints. Proceedings of Lunar and Planetary Science 22:3–20

Figowy S, Dubacq B, Noël Y, d'Arco P (2020) Partitioning of chromium between garnet and clinopyroxene: first principles modelling versus metamorphic assemblages. European Journal of Mineralogy 32:387–403, DOI 10.5194/ejm-32-387-2020

Figowy S, Dubacq B, D'Arco P (2021) Crystal chemistry and partitioning of halogens in hydrous silicates. Contributions to Mineralogy and Petrology 176(12):100, DOI 10.1007/s00410-021-01860-y

Gale JD (1997) GULP: A computer program for the symmetry-adapted simulation of solids. J Chem Soc, Faraday Trans 93:629–637, DOI 10.1039/A606455H

Gale JD, Rohl AL (2003) The General Utility Lattice Program (GULP). Molecular Simulation 29(5):291–341, DOI 10.1080/0892702031000104887

Ghiorso M (1984) Activity/composition relations in the ternary feldspars. Contributions to Mineralogy and Petrology 87:282–296, DOI 10.1007/BF00373061

Goldsmith JR, Newton RC (1974) The Feldspars, Manchester University Press, chap An experimental determination of the alkali feldspar solvus, pp 337–359

Harlow GE, Brown GE (1980) Low albite: An X-Ray and neutron diffraction study. American Mineralogist 65:986–995, URL https://pubs.geoscienceworld.org/ammin/article-pdf/65/9-10/986/4215751/am65_986.pdf

Hayward SA, Salje EKH (1996) Displacive phase transition in anorthoclase; the "plateau effect" and the effect of T1-T2 ordering on the transition temperature. American Mineralogist 81(11-12):1332–1336, DOI 10.2138/am-1996-11-1204

Holland T, Powell R (1992) Plagioclase feldspars: activity-composition relations based upon Darken's quadratic formalism and Landau theory. American Mineralogist 77(1-2):53–61

Holland T, Powell R (1996) Thermodynamics of order-disorder in minerals .1. Symmetric formalism applied to minerals of fixed composition. American Mineralogist 81(11-12):1413–1424, DOI 10.2138/am-1996-11-1214

Holland T, Powell R (2003) Activity-composition relations for phases in petrological calculations: an asymmetric multicomponent formulation. Contributions to Mineralogy and Petrology 145, 4:492–501, DOI 10.1007/s00410-003-0464-z

Holland TJB, Green ECR, Powell R (2022) A thermodynamic model for feldspars in $KAlSi_3O_8$-$NaAlSi_3O_8$-$CaAl_2Si_2O_8$ for mineral equilibrium calculations. Journal of Metamorphic Geology 40(4):587–600, DOI 10.1111/jmg.12639

Jin S, Xu H (2017) Solved: The enigma of labradorite feldspar with incommensurately modulated structure:. American Mineralogist 102(1):21–32, DOI 10.2138/am-2017-5807

Jin S, Xu H, Lee S (2021) Revisiting the Bøggild Intergrowth in Iridescent Labradorite Feldspars: Ordering, Kinetics, and Phase Equilibria. Minerals 11(7), DOI 10.3390/min11070727

Kerrick D, Darken L (1975) Statistical thermodynamic models for ideal oxide and silicate solid solutions, with application to plagioclase. Geochimica et Cosmochimica Acta 39(10):1431–1442, DOI 10.1016/0016-7037(75)90122-2

Kroll H, Bambauer HU, Pentinghaus H (2020) Na-feldspar: temperature, pressure and the state of order. European Journal of Mineralogy 32(4):427–441, DOI 10.5194/ejm-32-427-2020

Lanari P, Duesterhoeft E (2018) Modeling metamorphic rocks using equilibrium thermodynamics and internally consistent databases: Past achievements, problems and perspectives. Journal of Petrology 60(1):19–56, DOI 10.1093/petrology/egy105

Lowitzer S, Wilson D, Winkler B, Milman V, Gale J (2008) Defect properties of albite - a combined empirical potential and density functional theory study. Physics and Chemistry of Minerals 35, DOI 10.1007/s00269-007-0204-4

Luth W, Tuttle O (1966) The alkali feldspar solvus in the system Na_2O-K_2O-Al_2O_3-SiO_2-H_2O. American Mineralogist 51(9-10):1359–1373

Malcherek T, Carpenter MA, Kroll H, Salje EKH (1999) Cation ordering in $BaAl_2Ge_2O_8$-feldspar: implications for the phase transition in anorthite. Physics and Chemistry of Minerals 26:354–366, DOI 10.1007/s002690050195

Marquardt DW (1963) An algorithm for least-squares estimation of nonlinear parameters. Journal of the Society for Industrial and Applied Mathematics 11(2):pp. 431–441, URL http://www.jstor.org/stable/2098941

McConnell J (1974) The feldspars, Manchester University Press, chap Analysis of the time-temperature-transformation behaviour of the plagioclase feldspars, pp 460–477

Meyre C, De Capitani C, Partzsch JH (1997) A ternary solid solution model for omphacite and its application to geothermobarometry of eclogites from the Middle Adula nappe (Central Alps, Switzerland). Journal of Metamorphic Geology 15(6):687–700, DOI 10.1111/j.1525-1314.1997.00042.x

Myers E (1999) Al/Si ordering in silicate minerals. PhD thesis, University of Cambridge.

Myers E, Heine V, Dove M (1998) Thermodynamics of Al/Al avoidance in the ordering of Al/Si tetrahedral framework structures. Physics and Chemistry of Minerals 25:457–464, DOI 10.1007/s002690050136

Namur O, Charlier B (2017) Silicate mineralogy at the surface of Mercury. Nature Geoscience 10:9–13, DOI 10.1038/ngeo2860

Namur O, Charlier B, Pirard C, Hermann J, Liégeois JP, Auwera JV (2011) Anorthosite formation by plagioclase flotation in ferrobasalt and implications for the lunar crust. Geochimica et Cosmochimica Acta 75(17):4998 – 5018, DOI 10.1016/j.gca.2011.06.013

Namur O, Charlier B, Toplis M, Vander Auwera J (2012) Prediction of plagioclase-melt equilibria in anhydrous silicate melts at 1-atm. Contributions to Mineralogy and Petrology 163:133–150, 10.1007/s00410-011-0662-z

Orville PM (1963) Alkali ion exchange between vapor and feldspar phases. American Journal of Science 261(3):201–237, DOI 10.2475/ajs.261.3.201

Orville PM (1972) Plagioclase cation exchange equilibria with aqueous chloride solution; results at 700 degrees C and 2000 bars in the presence of quartz. American Journal of Science 272(3):234–272, DOI 10.2475/ajs.272.3.234

Phillips BL, Kirkpatrick RJ, Carpenter MA (1992) Investigation of short-range Al,Si order in synthetic anorthite by 29Si MAS NMR spectroscopy. American Mineralogist 77(5-6):484–494, https://pubs.geoscienceworld.org/ammin/article-pdf/77/5-6/484/4218024/am77_484.pdf

Powell R, Holland T (1993) On the formulation of simple mixing models for complex phases. American Mineralogist 78(11-12):1174–1180

Prewitt CT, Sueno S, Papike JJ (1976) The crystal structures of high albite and monalbite at high temperatures. American Mineralogist 61(11-12):1213–1225, https://pubs.geoscienceworld.org/msa/ammin/article-pdf/61/11-12/1213/4180075/am61_1213.pdf

Redfern SAT, Salje E (1987) Thermodynamics of plagioclase II: Temperature evolution of the spontaneous strain at the $I\bar{1} - P\bar{1}$ phase transition in anorthite. Physics and Chemistry of Minerals 14(2):189–195, DOI 10.1007/BF00308224

Sainz-Diaz CI, Hernández-Laguna A, Dove MT (2001) Modeling of dioctahedral 2:1 phyllosilicates by means of transferable empirical potentials. Physics and Chemistry of Minerals 28:130–141, DOI 10.1007/s002690000139

Salje E (1985) Thermodynamics of sodium feldspar I: Order parameter treatment and strain induced coupling effects. Physics and Chemistry of Minerals 12:93–98, DOI 10.1007/BF01046833

Salje E (1987) Thermodynamics of plagioclases I: Theory of the $I\bar{1} - P\bar{1}$ phase transition in anorthite and Ca-rich plagioclases. Physics and Chemistry of Minerals 14(2):181–188, DOI 10.1007/BF00308223

Salje E, Kuscholke B, Wruck B, Kroll H (1985) Thermodynamics of sodium feldspar II: Experimental results and numerical calculations. Physics and Chemistry of Minerals 12:99–107, DOI 10.1007/BF01046834

Schliestedt M, Johannes W (1990) Cation exchange equilibria between plagioclase and aqueous chloride solution at 600 to 700 °C and 2 to 5 kbar. European Journal of Mineralogy 2(3):283–295, DOI 10.1127/ejm/2/3/0283

Thompson J, Waldbaum DR (1969) Mixing properties of sanidine crystalline solutions: Iii. calculations based on two phase data. American Mineralogist 84:811–839

Tribaudino M, Gatta GD, Aliatis I, Bersani D, Lottici PP (2018) Al—Si ordering in albite: A combined single-crystal X-ray diffraction and Raman spectroscopy study. Journal of Raman Spectroscopy 49(12):2028–2035, DOI 10.1002/jrs.5490

Vidal O, De Andrade V, Lewin E, Munoz M, Parra T, Pascarelli S (2006) P-T-deformation-Fe^{3+}/Fe^{2+} mapping at the thin section scale and comparison with XANES mapping: application to a garnet-bearing metapelite from the Sambagawa metamorphic belt (Japan). Journal of Metamorphic Geology 24(7):669–683, DOI 10.1111/j.1525-1314.2006.00661.x

Vinograd VL, Putnis A (1999) The description of Al, Si ordering in aluminosilicates using the cluster variation method. American Mineralogist 84(3):311–324, DOI 10.2138/am-1999-0314

Vinograd VL, Putnis A (2001) A two-dimensional spin model of Al/Si order in feldspars: visualization of short-range and long-range order. European Journal of Mineralogy 13(2):273–288, DOI 10.1127/0935-1221/01/0013-0273

Vinograd VL, Sluiter MH (2006) Thermodynamics of mixing in pyrope-grossular, $Mg_3Al_2Si_3O_{12}$-$Ca_3Al_2Si_3O_{12}$, solid solution from lattice dynamics calculations and Monte Carlo simulations. American Mineralogist 91(11-12):1815–1830, DOI 10.2138/am.2006.2140

Vinograd VL, Putnis A, Kroll H (2001) Structural discontinuities in plagioclase and constraints on mixing properties of the low series: a computational study. Mineralogical Magazine 65(1):1–31, DOI 10.1180/002646101550073

Vinograd VL, Gale J, Winkler B (2007) Thermodynamics of mixing in diopside–jadeite, $CaMgSi_2O_6$–$NaAlSi_2O_6$ solid solution from static lattice energy calculations. Physics and Chem-

istry of Minerals 34:713–725, 10.1007/s00269-007-0189-z
Vinograd VL, Dymshits A, Winkler B, Bobrov A (2011) Computer simulation of Na-bearing majoritic garnet. Doklady Earth Sciences 441:1508–1511, DOI 10.1134/S1028334X11110092
Winkler B, Dove MT, Leslie M (1991) Static lattice energy minimization and lattice dynamics calculations on aluminosilicate minerals. American Mineralogist 76(3-4):313–331, URL `http://ammin.geoscienceworld.org/content/76/3-4/313.short`